AD-A243 378

PL-TR-91-2171

NWRA-CR-91-R072

AN INVESTIGATION OF METHODS FOR UPDATING IONOSPHERIC SCINTILLATION MODELS USING TOPSIDE *IN-SITU* PLASMA DENSITY MEASUREMENTS

James A. Secan
Northwest Research Associates, Inc.
P.O. Box 3027
Bellevue, Washington 98009

15 May 1991

Scientific Report No. 1

Approved for public release; distribution unlimited

DTIC
ELECTE
OCT 16 1991
S B D

PHILLIPS LABORATORY
AIR FORCE SYSTEMS COMMAND
HANSCOM AIR FORCE BASE, MASSACHUSETTS 01731-5000

91-13288

"This technical report has been reviewed and is approved for publication"

EDWARD J. WEBER
Contract Manager

WILLIAM K. VICKERY
Branch Chief

FOR THE COMMANDER

ROBERT A. SKRIVANEK
Division Director

This report has been reviewed by the ESD Public Affairs Office (PA) and is releasable to the National Technical Information Service (NTIS).

Qualified requestors may obtain additional copies from the Defense Technical Information Center. all others should apply to the National Technical Information Service.

If your address has changed, or if you wish to be removed from the mailing list, or if the addressee is no longer employed by your organization, please notify GL/IMA, Hanscom AFB, MA 01731. This will assist us in maintaining a current mailing list.

Do not return copies of this report unless contractual obligations or notices on a specific document requires that it be returned.

REPORT DOCUMENTATION PAGE

Form Approved
OMB No. 0704-0188

Public reporting burden for this collection of information is estimated to average 1 hour per response, including the time for reviewing instructions, searching existing data sources, gathering and maintaining the data needed, and completing and reviewing the collection of information. Send comments regarding this burden estimate or any other aspect of this collection of information, including suggestions for reducing this burden to Washington Headquarters Services, Directorate for information Operations and Reports, 1215 Jefferson Davis Highway, Suite 1204, Arlington, VA 22202-4302, and to the Office of Management and Budget, Paperwork Reduction Project (0704-0188), Washington, DC 20503

1. AGENCY USE ONLY (Leave blank)	2. REPORT DATE	3. REPORT TYPE AND DATES COVERED
	15 May 1991	Scientific No. 1, 1 May 90 - 30 Apr 91

4. TITLE AND SUBTITLE
An Investigation of Methods for Updating Ionospheric Scintillation Models Using Topside *In-Situ* Plasma Density Measurements

5. FUNDING NUMBERS
F19628-90-C-0072
PE 35160F
PR DMSS
TA01
WUAB

6. AUTHOR(S)
Secan, James A.

7. PERFORMING ORGANIZATION NAME(S) AND ADDRESS(ES)
Northwest Research Associaties, Inc.
P.O. Box 3027
Bellevue, WA 98009

8. PERFORMING ORGANIZATION REPORT NUMBER
NWRA-CR-91-R072

9. SPONSORING/MONITORING AGENCY NAME(S) AND ADDRESS(ES)
Phillips Laboratory
Hanscom AFB, MA 01731-5000

Contract Manager: Edward Weber/LIS

10. SPONSORING/MONITORING AGENCY REPORT NUMBER
PL-TR-91-2171

11. SUPPLEMENTARY NOTES

12a. DISTRIBUTION/AVAILABILITY STATEMENT
approved for public release;
distribution unlimited

12b. DISTRIBUTION CODE

13. ABSTRACT *(Maximum 200 words)*

Modern military communication, navigation, and surveillance systems depend on reliable, noise-free transionospheric radio-frequency channels. They can be severely impacted by small-scale electron-density irregularities in the ionosphere, which cause both phase and amplitude scintillation. Basic tools used in planning and mitigation schemes are climatological in nature and thus may greatly over- and under-estimate the effects of scintillation in a given scenario. This report summarizes the results of the first year of a three-year investigation into the methods for updating ionospheric scintillation models using observations of ionospheric plasma-density irregularities measured by the DMSP Scintillation Meter (SM) sensor. Results are reported from the analysis of data from a campaign conducted in January 1990 near Tromso, Norway, in which near coincident *in-situ* plasma-density and transionospheric scintillation measurements were made. Estimates for the level of intensity and phase scintillation on a transionospheric UHF radio link in the early-evening auroral zone were calculated from DMSP SM data and compared to the levels actually observed.

14. SUBJECT TERMS	15. NUMBER OF PAGES
Ionosphere, Ionospheric Scintillation, Radiowave Scintillation, Defense Meteorology Satellite Program (DMSP)	58
	16. PRICE CODE

17. SECURITY CLASSIFICATION OF REPORT	18. SECURITY CLASSIFICATION OF THIS PAGE	19. SECURITY CLASSIFICATION OF ABSTRACT	20. LIMITATION OF ABSTRACT
Unclassified	Unclassified	Unclassified	SAR

TABLE OF CONTENTS

Page

1. Introduction 1

2. Analysis of SSIES/AIO/EISCAT 1990 Campaign Data 2

3. Conclusion 13

References 13

Appendix A. Summary Data Plots for the 1990 SSIES/AIO Campaign 14

Appendix B. Data and PDS Plots for 17 January 1990 30

COPY INSPECTED 4

Accession For
NTIS GRA&I ☑
DTIC TAB ☐
Unannounced ☐
Justification
By
Distribution/
Availability Codes
Dist | Avail and/or Special
A-1

LIST OF FIGURES

Figure	Caption	Page
1	Geometry of the SSIES/AIO experiment for 17 January 1990. The locations of the AIO-AFSATCOM 300-km ionospheric penetration point (IPP) and the SSIES 300-km field-line footprint are shown for the center times of data sets used in the analysis. The time/location of closest approach is indicated by horizontal bars on the two location traces. The circled numbers are the numbers for the data sets used in this report.	4
2	The variation of the total ion density from the SSIES SM sensor (top plot), the horizontal cross-track ion drift velocity from the DM sensor (U_h) (middle plot), and the vertical cross-track velocity from the DM sensor (U_v) (bottom plot) with time and location along the DMSP orbit. The circled numbers in the top plot correspond to the locations identified in Figure 1. (Note: A positive value for U_h corresponds to flow in the sunward direction.)	6
3	The slope of the *in-situ* spectrum (q) (top plot) and the estimated C_kL (bottom plot) derived from the SSIES SM density data plotted for the same time period covered in Figure 2.	7
4	Detrended intensity (upper plot) and phase (middle plot) from the AIO-AFSATCOM link, and the *in-situ* ion density data covering the locations shown in Figure 1. The density data have been plotted in reverse-time order and the scales of the AIO-AFSATCOM data adjusted so that the data sets are nearly aligned along geomagnetic latitude. The circled numbers mark the center times of the data sets used to generate the various parameters in the analysis, and they correspond to the numbers in previous figures.	8
5	Values of σ_ϕ (top plot) and S_4 (middle plot) generated from the SSIES data (squares), the AIO-AFSATCOM data (triangles), and the WBMOD model (pluses). The bottom plot is a repeat of the SSIES density plot shown in Figure 4.	9
6	Values of T (top plot) and p (middle plot) generated from the SSIES data (squares), the AIO-AFSATCOM data (triangles), and the WBMOD model (pluses). The bottom plot shows C_kL estimates from the SSIES data (squares), the AIO-AFSATCOM σ_ϕ (diamonds) and S_4 (triangles) data, and the WBMOD model (pluses). All plots are as a function of "reverse" SSIES time (as in the plots in Figures 4 and 5).	10

Figure	Caption	Page
7	The variation of total ion density through the northern-hemisphere, pre-midnight auroral ionosphere for four sequential DMSP passes. The arrow in the AIO-REV plot shows the location of the AIO-AFSATCOM scintillation "boundary."	12
A-1	Geometry of the SSIES/AIO experiment for 17 January 1990. The locations of the AIO-AFSATCOM 300-km ionospheric penetration point (IPP) and the SSIES 300-km field-line footprint are shown. The time/location of closest approach is indicated by time tags near the center of each location trace.	15
A-2	The variation of the total ion density from the SSIES SM sensor (top plot), the horizontal cross-track ion drift velocity from the DM sensor (U_h) (middle plot), and the vertical cross-track velocity from the DM sensor (U_v) (bottom plot) with time and location along the DMSP orbit for 17 January 1990. (Note: A positive value for U_h corresponds to flow in the sunward direction.)	16
A-3	The slope (q) (top plot) and strength (T_1) (bottom plot) of the *in-situ* spectrum derived from the (detrended) SSIES SM density data plotted for the same time period covered in Figure A-2.	17
A-4	Geometry of the SSIES/AIO experiment for 23 January 1990. The locations of the AIO-AFSATCOM 300-km ionospheric penetration point (IPP) and the SSIES 300-km field-line footprint are shown. The time/location of closest approach is indicated by time tags near the center of each location trace.	18
A-5	The variation of the total ion density from the SSIES SM sensor (top plot), the horizontal cross-track ion drift velocity from the DM sensor (U_h) (middle plot), and the vertical cross-track velocity from the DM sensor (U_v) (bottom plot) with time and location along the DMSP orbit for 23 January 1990. (Note: A positive value for U_h corresponds to flow in the sunward direction.)	19
A-6	The slope (q) (top plot) and strength (T_1) (bottom plot) of the *in-situ* spectrum derived from the (detrended) SSIES SM density data plotted for the same time period covered in Figure A-5.	20

Figure	Caption	Page
A-7	Geometry of the SSIES/AIO experiment for 24 January 1990. The locations of the AIO-AFSATCOM 300-km ionospheric penetration point (IPP) and the SSIES 300-km field-line footprint are shown. The time/location of closest approach is indicated by time tags near the center of each location trace.	21
A-8	The variation of the total ion density from the SSIES SM sensor (top plot), the horizontal cross-track ion drift velocity from the DM sensor (U_h) (middle plot), and the vertical cross-track velocity from the DM sensor (U_v) (bottom plot) with time and location along the DMSP orbit for 24 January 1990. (Note: A positive value for U_h corresponds to flow in the sunward direction.)	22
A-9	The slope (q) (top plot) and strength (T_1) (bottom plot) of the *in-situ* spectrum derived from the (detrended) SSIES SM density data plotted for the same time period covered in Figure A-8.	23
A-10	Geometry of the SSIES/AIO experiment for 25 January 1990. The locations of the AIO-AFSATCOM 300-km ionospheric penetration point (IPP) and the SSIES 300-km field-line footprint are shown. The time/location of closest approach is indicated by time tags near the center of each location trace.	24
A-11	The variation of the total ion density from the SSIES SM sensor (top plot), the horizontal cross-track ion drift velocity from the DM sensor (U_h) (middle plot), and the vertical cross-track velocity from the DM sensor (U_v) (bottom plot) with time and location along the DMSP orbit for 25 January 1990. (Note: A positive value for U_h corresponds to flow in the sunward direction.)	25
A-12	The slope (q) (top plot) and strength (T_1) (bottom plot) of the *in-situ* spectrum derived from the (detrended) SSIES SM density data plotted for the same time period covered in Figure A-11.	26
A-13	Geometry of the SSIES/AIO experiment for 28 January 1990. The locations of the AIO-AFSATCOM 300-km ionospheric penetration point (IPP) and the SSIES 300-km field-line footprint are shown. The time/location of closest approach is indicated by time tags near the center of each location trace.	27

Figure	Caption	Page
A-14	The variation of the total ion density from the SSIES SM sensor (top plot), the horizontal cross-track ion drift velocity from the DM sensor (U_h) (middle plot), and the vertical cross-track velocity from the DM sensor (U_v) (bottom plot) with time and location along the DMSP orbit for 28 January 1990. (Note: A positive value for U_h corresponds to flow in the sunward direction.)	28
A-15	The slope (q) (top plot) and strength (T_1) (bottom plot) of the *in-situ* spectrum derived from the (detrended) SSIES SM density data plotted for the same time period covered in Figure A-14.	29
B-1	Detrended total ion density from the DMSP SSIES SM sensor (top plot) and the PDS generated from this data sample (lower plot) for data point no. 1 as identified in Table 3. The straight line plotted over the PDS is the power-law fit used to estimate T_1 and q.	31
B-2	Detrended phase from the AIO-AFSATCOM link (top plot) and the PDS generated from this data sample (lower plot) for data point no. 1 as identified in Table 3. The straight line plotted over the PDS is the power-law fit used to estimate T and p.	32
B-3	The same as plot B-1 (SSIES data) for data point no. 2.	33
B-4	The same as plot B-2 (AIO-AFSATCOM data) for data point no. 2.	34
B-5	The same as plot B-1 (SSIES data) for data point no. 3.	35
B-6	The same as plot B-2 (AIO-AFSATCOM data) for data point no. 3.	36
B-7	The same as plot B-1 (SSIES data) for data point no. 4.	37
B-8	The same as plot B-2 (AIO-AFSATCOM data) for data point no. 4.	38
B-9	The same as plot B-1 (SSIES data) for data point no. 5.	39
B-10	The same as plot B-2 (AIO-AFSATCOM data) for data point no. 5.	40
B-11	The same as plot B-1 (SSIES data) for data point no. 6.	41
B-12	The same as plot B-2 (AIO-AFSATCOM data) for data point no. 6.	42
B-13	The same as plot B-1 (SSIES data) for data point no. 7.	43
B-14	The same as plot B-2 (AIO-AFSATCOM data) for data point no. 7.	44

Figure	Caption	Page
B-15	The same as plot B-1 (SSIES data) for data point no. 8.	45
B-16	The same as plot B-2 (AIO-AFSATCOM data) for data point no. 8.	46
B-17	The same as plot B-1 (SSIES data) for data point no. 9.	47
B-18	The same as plot B-2 (AIO-AFSATCOM data) for data point no. 9.	48

LIST OF TABLES

Table	Caption	Page
1	Dates and time periods covered by the January 1990 campaign.	2
2	Procedures for calculating T_1 and q from DMSP SSIES Scintillation Meter data.	3
3	Center times (GMT) of the SSIES and AIO-AFSATCOM data segments for the 17 January 1990 (RR#1) data set. The time in parenthesis is seconds since midnight.	3

PREFACE

This report summarizes the work completed during the first year of an investigation into methods for updating computer-based models of ionospheric scintillation using *in-situ* observations of the ionosphere from the DMSP SSIES sensors. This work is part of a larger effort with an overall objective of providing the USAF Air Weather Service with the capability of observing ionospheric scintillations, and the plasma density irregularities that cause the scintillations, in near real-time and updating models of ionospheric scintillation with these observations.

1. Introduction

Many modern military systems used for communications, command and control, navigation, and surveillance depend on reliable and relatively noise-free transmission of radiowave signals through the earth's ionosphere. Small-scale irregularities in the ionospheric density can cause severe distortion, known as radiowave scintillation, of both the amplitude and phase of these signals. A basic tool used in estimating these effects on systems is a computer program, WBMOD, based on a single-scatter phase-screen propagation model and a number of empirical models of the global morphology of ionospheric density irregularities. An inherent weakness of WBMOD is that the irregularity models provide median estimates for parameters with large dynamic ranges, which can lead to large under- and over-estimation of the effects of the ionospheric irregularities on a system.

One solution to this problem, at least for near real-time estimates, is to update the WBMOD irregularity models with observations of the various parameters modeled. One proposed source for these observations is from the *in-situ* plasma density monitor to be flown on the Defense Meteorology Satellite Program (DMSP) satellites. A previous study assessed the applicability of these data to real-time updates of the WBMOD models[1]. (This study will be denoted the assessment study throughout this report.) In the present study, techniques developed in the assessment study for characterizing scintillation level in the high-latitude ionosphere will be improved, and further techniques for using these data to characterize scintillation levels in the equatorial and mid latitude ionosphere will be developed.

During the assessment study[1], a set of data was collected in a multi-instrument experiment conducted in the auroral zone near Tromso, Norway, during the month of January 1988. Scintillation measurements were made from the USAF Airborne Ionospheric Observatory (AIO) aircraft on a propagation path to one of the USAF AFSATCOM satellites timed and located to coincide with a DMSP F8 satellite pass. At nearly the same time, the EISCAT incoherent radar (located near Tromso) was measuring the background electron density profiles and *in-situ* plasma drifts up to an altitude of roughly 600 km along a geomagnetic meridian. Data from one pass in that data set were analyzed in detail in the assessment study, which found that the estimates of the level of intensity scintillation calculated from the DMSP *in-situ* plasma density measurements matched the levels observed on the AIO-AFSATCOM link fairly well.

That campaign was run just after solar minimum, so the background plasma-density levels were fairly low. It was decided to repeat the experiments later in the cycle when the density levels would be much higher. The second data collection campaign was conducted in January 1990 when the sunspot number was roughly a factor of three higher that in January 1988, and the observed plasma densities at DMSP altitude were a factor of two to four higher than those observed in the earlier campaign. In addition, since the DMSP F9 satellite had been launched with an SSIES instrument, data were collected from the pre-midnight sector from F9 as well as from the early evening sector from F8.

This report summarizes the progress of this study during the first year of this project, which focused on analysis of the data collected during the January 1990 campaign.

2. Analysis of SSIES/AIO/EISCAT 1990 Campaign Data

The time periods covered by the 1990 campaign are listed in Table 1. Summary plots for each pass are included in Appendix A. The summary plots include the following for each pass:

1. A plot of the 300-km ionospheric penetration point (IPP) location for the AIO-AFSAT link and the 300-km field-line footprint for the SSIES observations around the time of nearest approach.

2. Plots of the *in situ* total ion density from the SSIES Scintillation Meter (SM) and the two cross-track *in situ* ion drift-velocity components from the Drift Meter (DM) for a 5-minute period centered on the time of nearest approach.

3. Plots of the spectral slope (q) and strength (T_1) derived from fits to the power-density spectrum (PDS) generated from the *in situ* density. These parameters were generated from 256-point data samples using procedures summarized in Table 2 which were developed in the assessment study.

Table 1. Dates and time periods covered by the January 1990 campaign.

Date	AIO RR#	DMSP	Time Period(DMSP)	Time Period (AIO)
17 Jan	1	F8	18:31:28 - 18:36:28	18:19:28 - 18:43:52
23 Jan	3	F9	21:50:59 - 21:55:59	21:57:21 - 22:07:45
24 Jan	4	F8	18:40:28 - 18:45:28	18:33:24 - 18:52:12
25 Jan	5	F8	18:27:24 - 18:32:24	18:22:34 - 18:38:34
28 Jan	7	F9	21:48:47 - 21:53:47	21:43:56 - 21:57:08

Intensity and phase data from the AIO-AFSATCOM VHF link (250 MHz) have been received for the time intervals listed in Table 3. A detailed analysis of data from the pass on 17 January 1990 (RR #1) has been completed, and the results of the analysis will be described in this report. The remaining five days will be similarly analyzed during the second year of the project.

Figure 1 shows the relative positions of the AIO-AFSAT IPP and the SSIES 300-km footprint, the times at the ends of each data segment, and the location and time of nearest

Table 2. Procedures for calculating T_1 and q from DMSP SSIES Scintillation Meter data.

1. Detrend the ion density data by removing a background trend. This trend can be calculated from either a low-pass filter applied to the entire data set or a quadratic least-squares fit to each data sample (256 or 512 points).

2. Apply a time-domain window to the detrended data sample. The window of choice is a 30% split-bell cosine taper.

3. Use an FFT of the detrended, windowed data sample to calculate an estimate of the PDS ($\Phi_{\Delta N}$).

4. Smooth the PDS estimate. The smoothing function used is a five-point, centered function with binomial weights.

5. Use a linear least-squares fit to log(PDS) versus log(frequency) over the frequency range 0.3 to 5.0 Hz.

Table 3. Center times (GMT) of the SSIES and AIO-AFSAT data segments for the 17 January 1990 (RR#1) data set. The time in parenthesis is seconds since midnight.

Segment Number	SSIES	AIO-AFSATCOM
1	18:34:28 (66868)	18:20:28 (66028)
2	18:34:23 (66863)	18:23:16 (66196)
3	18:34:18 (66858)	18:26:04 (66364)
4	18:34:13 (66853)	18:28:52 (66532)
5	18:34:08 (66848)	18:31:40 (66700)
6	18:34:03 (66843)	18:34:28 (66868)
7	18:33:58 (66838)	18:37:16 (67036)
8	18:33:53 (66833)	18:40:04 (67204)
9	18:33:48 (66828)	18:42:52 (67372)

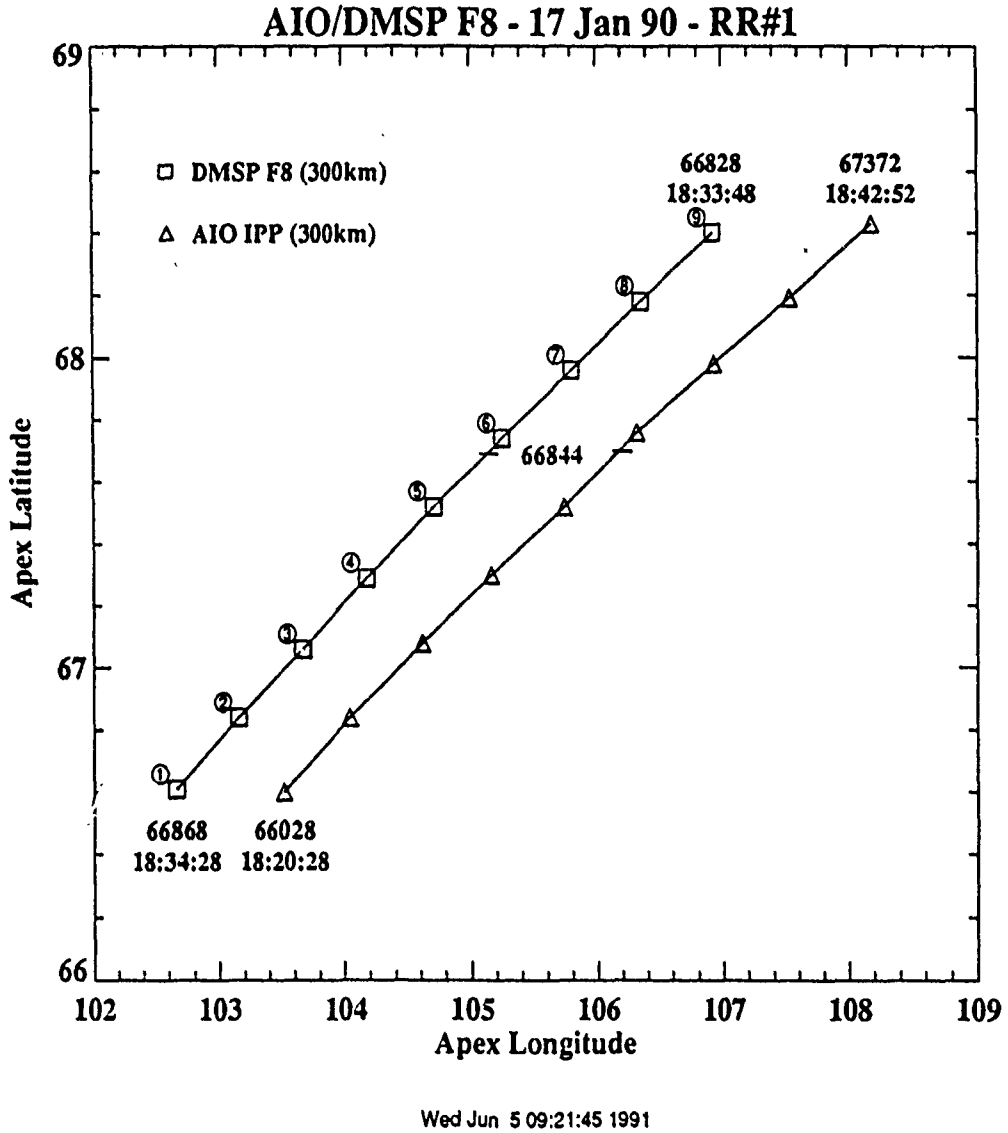

Figure 1. Geometry of the SSIES/AIO experiment for 17 January 1990. The locations of the AIO-AFSATCOM 300-km ionospheric penetration point (IPP) and the SSIES 300-km field-line footprint are shown for the center times of data sets used in the analysis. The time/location of closest approach is indicated by horizontal bars on the two location traces. The circled numbers are the numbers for the data sets used in this report.

approach (66844 seconds, indicated by a horizontal bar on both traces) for the 17 January pass. The symbols on this figure are plotted at locations corresponding to the center times of data subsets used to calculate spectra and scintillation indices. The circled numbers located near the SSIES symbols will be used to identify the various data segments in later plots. Table 3 lists the center times of the SSIES and AIO-AFSAT data sets corresponding to each of these numbers. (Note: The center times were selected to center each data segment between the AFSATCOM retune times, which occur every 168 seconds.) Plots of the detrended density data and the detrended phase data with their associated power-density spectra for each data segment can be found in Appendix B.

The SSIES SM and DM data for this pass are shown in Figure 2, with the data-segment locations indicated on the plot of total ion density from the SM sensor. The *in situ* spectral slope and the estimated C_kL calculated from these data are shown in Figure 3. The C_kL estimates were calculated from T_1 and q using procedures developed in the assessment study. A model for the background plasma-density profile was used to convert the *in-situ* C_k measurement to C_kL as the EISCAT-observed profiles are not yet available (see the Appendix in [1]). The profile model was fit to the plasma density measured at the satellite altitude by iteratively adjusting the peak density and a model adjustment parameter (α_0 in Eq. A-2 in the Appendix to [1]).

Figure 4 shows the detrended intensity and phase from the AIO-AFSAT link used in the analysis, along with the SSIES SM density data (note that the SM data are plotted in reverse-time order so that both the AIO-AFSAT and SM data are plotted with latitude increasing from left to right). Both the intensity and phase have been detrended using a 6-pole Butterworth low-pass filter with a 10-second (0.1 Hz) cutoff. The sharp spikes in the phase data occur at retune points, which are manifest in the phase data by sharp discontinuities in the slope of the phase variation. The AIO-AFSAT data segments used in this analysis are 81.92-second samples (4096 data points) centered between the retune spikes. Since the time between the spikes is 168 seconds, the "ringing" found in the vicinity of the spikes did not contaminate any of the data samples.

The C_kL estimates were used to calculate values of phase spectral parameters p and T and scintillation indices S_4 and σ_ϕ. These calculations were based on the power-law phase-screen theory used in the WBMOD scintillation model[2]. S_4 and σ_ϕ were calculated (in the time domain) from the detrended AIO-AFSAT intensity and phase data, respectively, and estimates of p and T were extracted from phase spectra. The AIO-AFSAT S_4 and σ_ϕ data were used to calculate estimates of C_kL, also using the WBMOD propagation theory. Finally, values for all parameters were calculated using the WBMOD scintillation model[3,4] based on the date, time, and location of the observations, as well as the sunspot number and K_p valid for those times. The results are shown in Figures 5 and 6. In Figure 5, all estimates of σ_ϕ (top plot) and S_4 (middle plot) are plotted as a function of "reverse" SSIES time (as in Figure 4) along with the SM sensor density data (repeated from Figure 4). All estimates of the phase spectral parameters (T and p) and of C_kL are plotted in Figure 6.

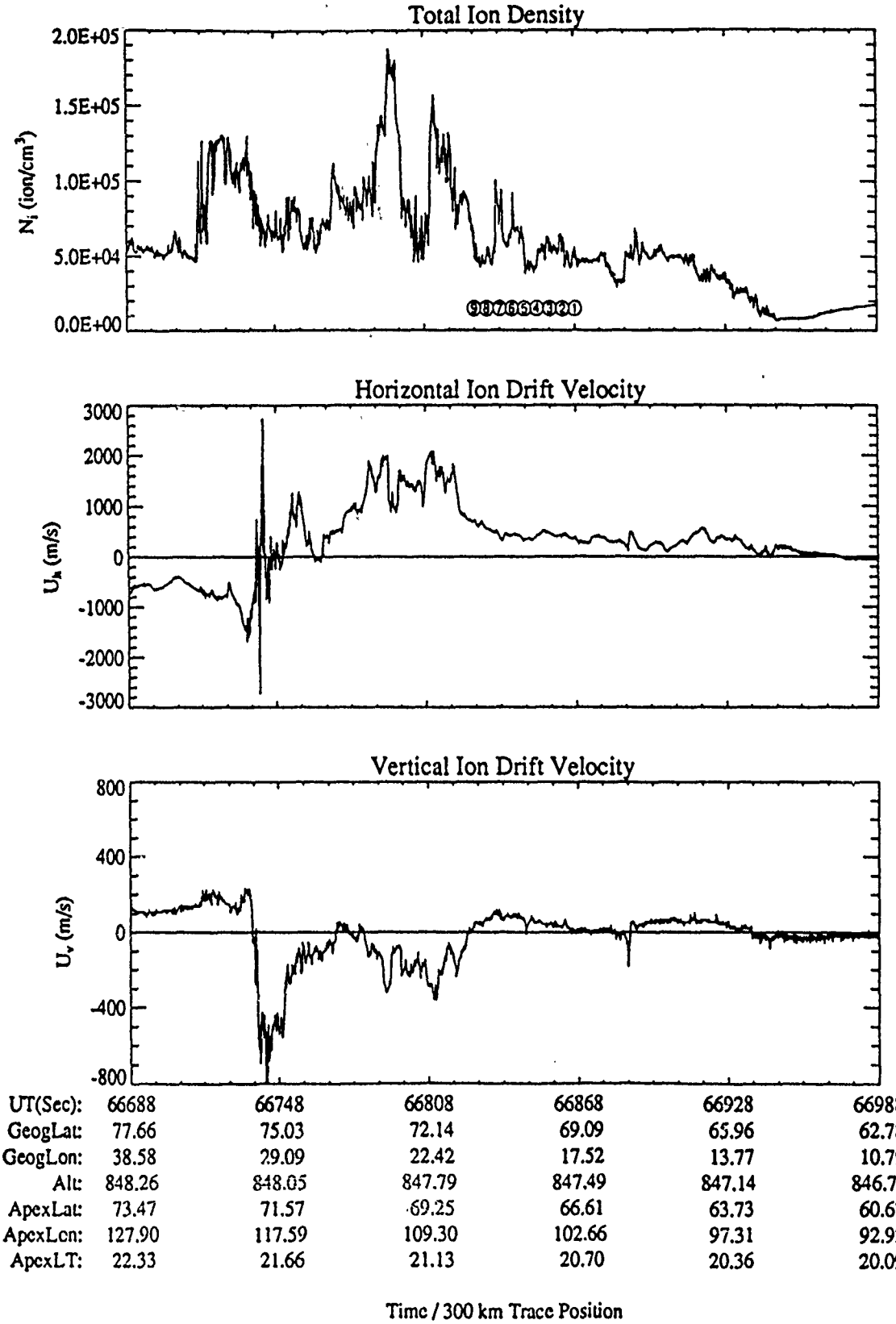

Figure 2. The variation of the total ion density from the SSIES SM sensor (top plot), the horizontal cross-track ion drift velocity from the DM sensor (U_h) (middle plot), and the vertical cross-track velocity from the DM sensor (U_v) (bottom plot) with time and location along the DMSP orbit. The circled numbers in the top plot correspond to the locations identified in Figure 1. (Note: A positive value for U_h corresponds to flow in the sunward direction.)

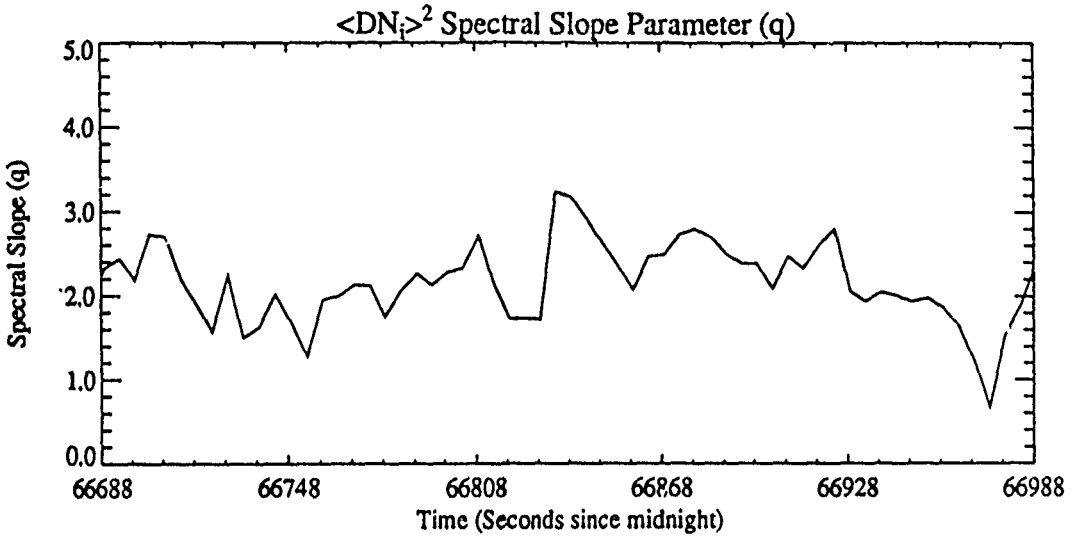

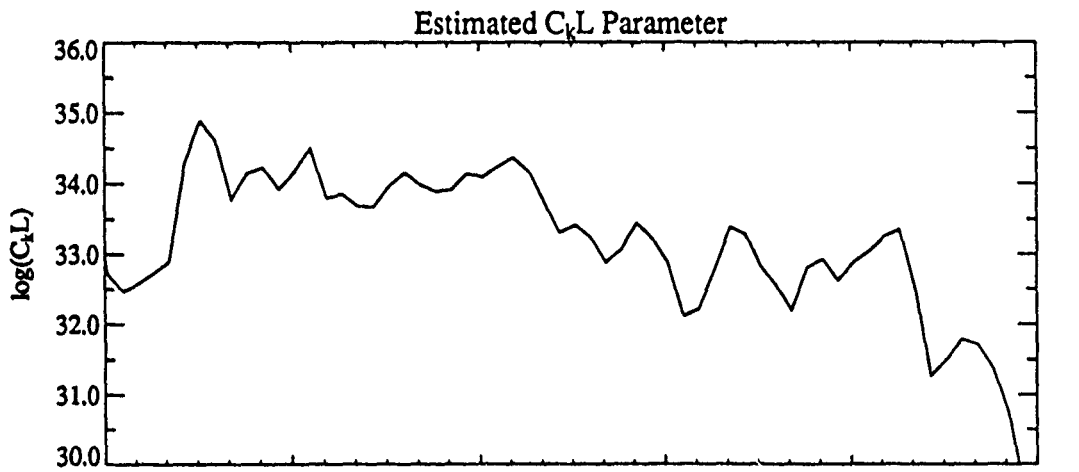

UT(Sec):	66688	66748	66808	66868	66928	66988
GeogLat:	36.74	33.61	30.50	27.44	24.42	21.48
GeogLon:	314.82	313.77	312.76	311.77	310.80	309.83
Alt:	910.63	903.18	896.03	889.22	882.80	876.78
ApexLat:	41.75	38.72	35.77	32.92	30.18	27.58
ApexLon:	36.53	34.84	33.19	31.54	29.90	28.23
ApexLT:	16.24	16.15	16.05	15.96	15.87	15.77

Time / 300 km Trace Position

Fri May 24 10:32:41 1991

Figure 3. The slope of the *in-situ* spectrum (q) (top plot) and the estimated C_kL (bottom plot) derived from the SSIES SM density data plotted for the same time period covered in Figure 2.

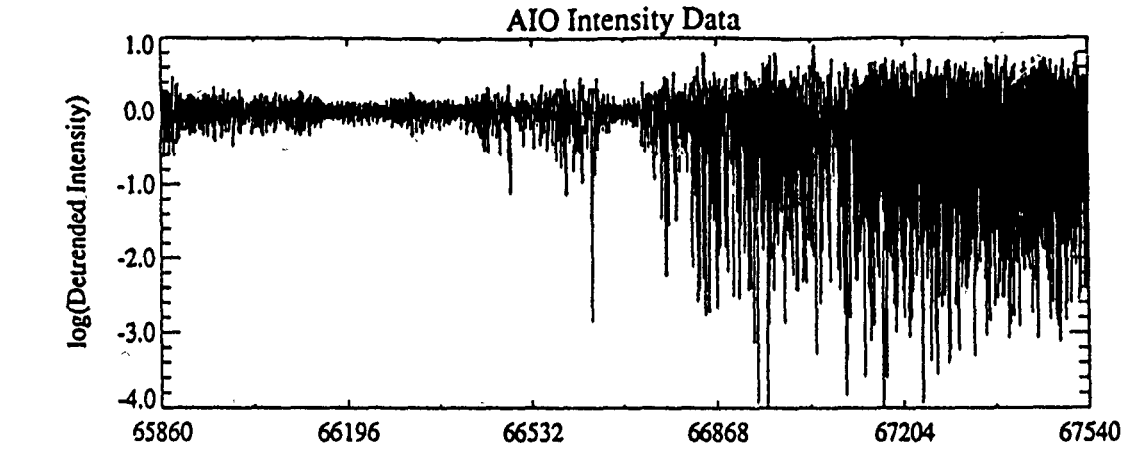

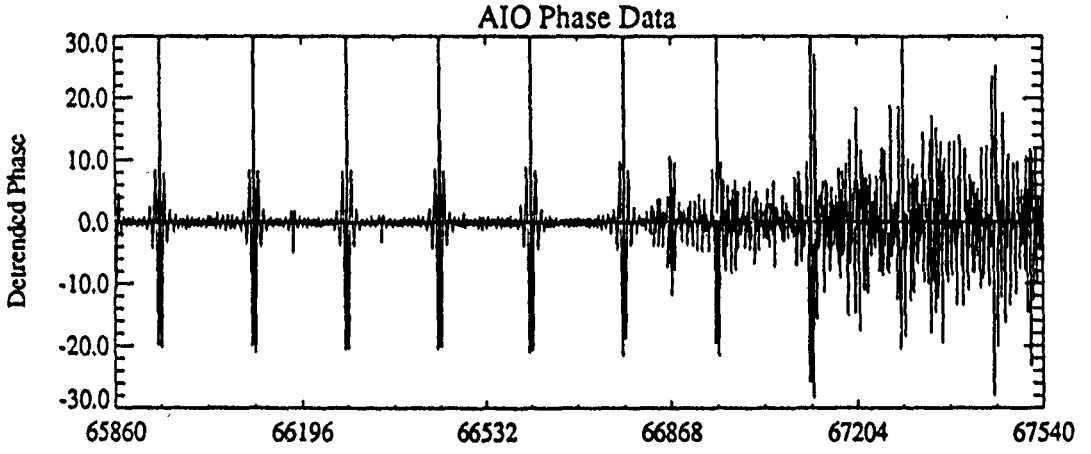

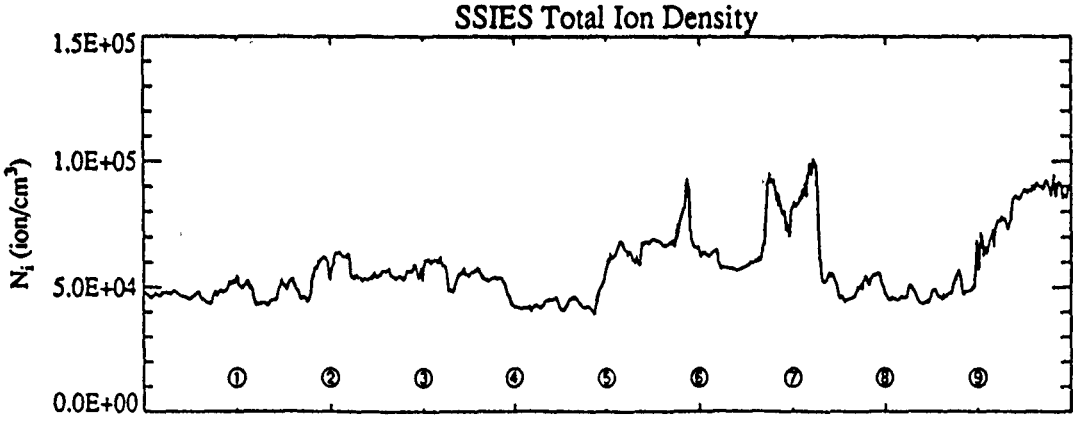

UT(Sec):	66873	66863	66853	66843	66833	66823
GeogLat:	68.83	69.35	69.86	70.37	70.88	71.39
GeogLon:	17.17	17.87	18.61	19.39	20.20	21.06
Alt:	847.46	847.51	847.57	847.62	847.67	847.72
ApexLat:	66.37	66.84	67.29	67.74	68.18	68.61
ApexLon:	102.17	103.16	104.18	105.25	106.35	107.50
ApexLT:	20.67	20.73	20.80	20.87	20.94	21.01

Time / 300 km Trace Position

Figure 4. Detrended intensity (upper plot) and phase (middle plot) from the AIO-AFSATCOM link, and the *in-situ* ion density data covering the locations shown in Figure 1. The density data have been plotted in reverse-time order and the scales of the AIO-AFSATCOM data adjusted so that the data sets are nearly aligned along geomagnetic latitude. The circled numbers mark the center times of the data sets used to generate the various parameters in the analysis, and they correspond to the numbers in previous figures.

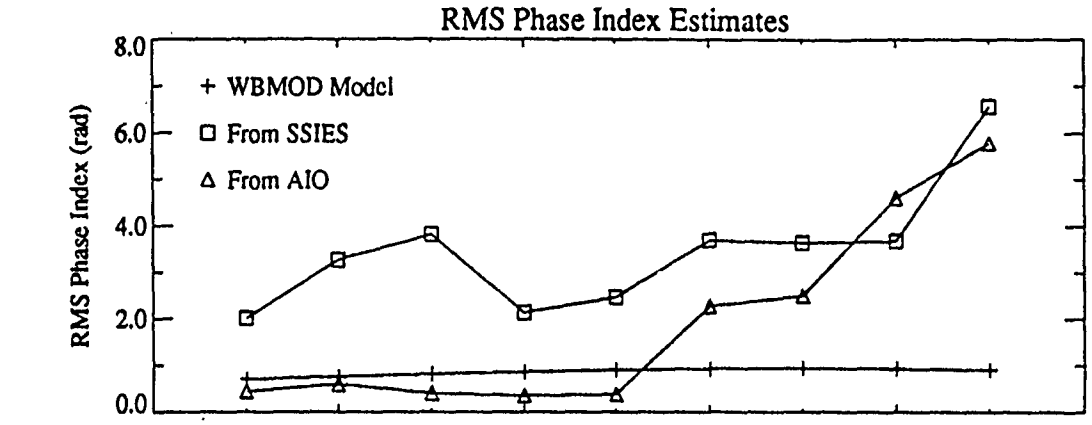

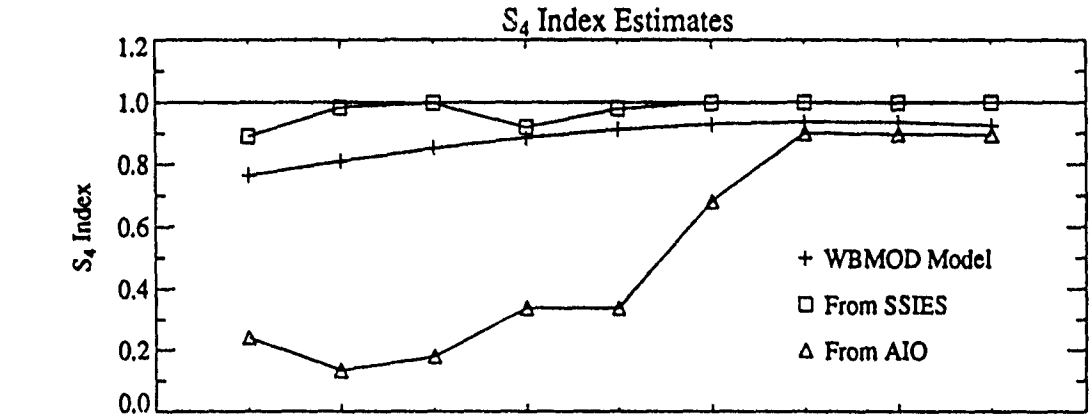

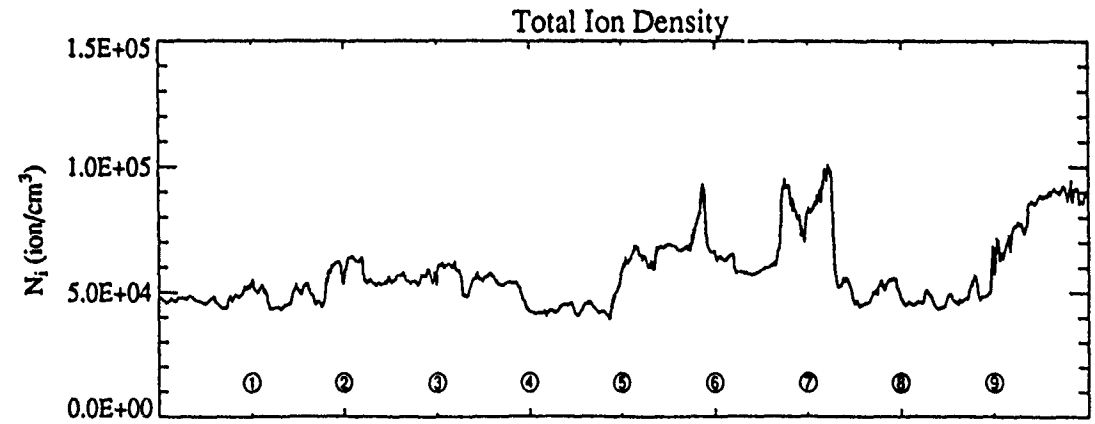

UT(Sec):	66873	66863	66853	66843	66833	66823
GeogLat:	68.83	69.35	69.86	70.37	70.88	71.39
GeogLon:	17.17	17.87	18.61	19.39	20.20	21.06
Alt:	847.46	847.51	847.57	847.62	847.67	847.72
ApexLat:	66.37	66.84	67.29	67.74	68.18	68.61
ApexLon:	102.17	103.16	104.18	105.25	106.35	107.50
ApexLT:	20.67	20.73	20.80	20.87	20.94	21.01

Time / 300 km Trace Position

Figure 5. Values of σ_ϕ (top plot) and S_4 (middle plot) generated from the SSIES data (squares), the AIO-AFSATCOM data (triangles), and the WBMOD model (pluses). The bottom plot is a repeat of the SSIES density plot shown in Figure 4.

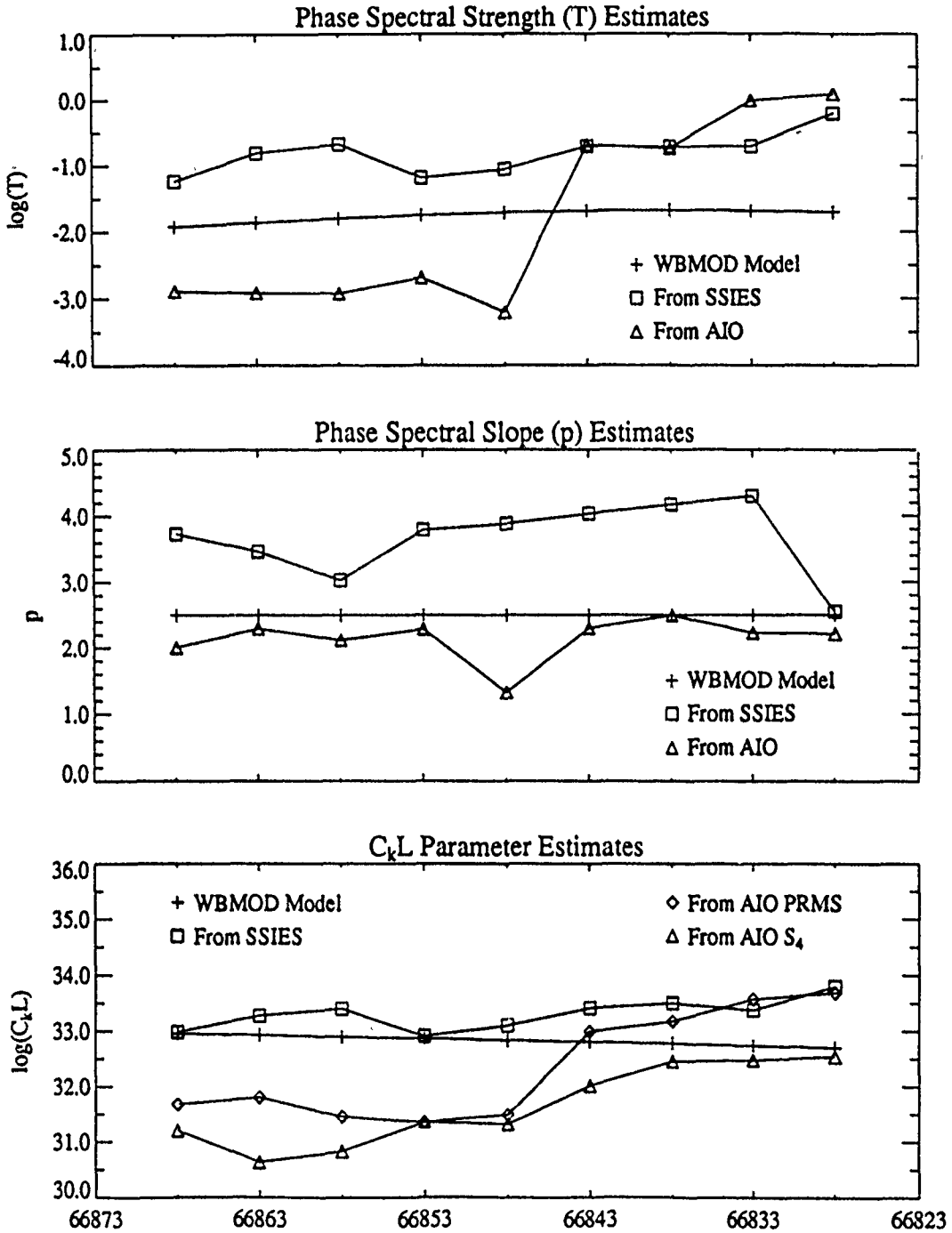

Figure 6. Values of T (top plot) and p (middle plot) generated from the SSIES data (squares), the AIO-AFSATCOM data (triangles), and the WBMOD model (pluses). The bottom plot shows C_kL estimates from the SSIES data (squares), the AIO-AFSATCOM σ_ϕ (diamonds) and S_4 (triangles) data, and the WBMOD model (pluses). All plots are as a function of "reverse" SSIES time (as in the plots in Figures 4 and 5).

In general, the results obtained from this data set are much less promising than those obtained from analysis of data from the 1988 campaign[1]. The parameters calculated from the SSIES data compare fairly well with those calculated from the AIO-AFSAT data at the high-latitude end of the latitude range covered by the data. The AIO-AFSAT data, however, appear to pass through a boundary roughly halfway through the data set which does not appear in the SSIES-derived parameters. Equatorward of this boundary, the comparison between the SSIES and the AIO-AFSAT parameters is fairly poor.

One possibility for this disagreement was that the boundary seen in the AIO-AFSAT data moved rapidly equatorward just prior to the SSIES pass. This would require a fairly high rate of movement (on the order of 5 km/sec), and was ruled out based on the low levels of geomagnetic activity prevalent throughout the period (K_p of 2 in the 1500-1800 GMT period and 2- in the 1800-2100 GMT period) and on the plots in Figure 7. Shown in these plots are the density from the SSIES SM sensor on four sequential passes through the northern-hemisphere post-midnight auroral zone. The pass being analyzed is the third plot from the top. The data have been plotted such that they cover roughly the same range of geomagnetic latitudes. As can be seen, the equatorward edge of the auroral ionosphere moves roughly one degree toward the equator between the first and second passes shown, and very little thereafter. In none of the four passes, covering the time interval 1507 GMT to 2020 GMT, was this boundary located near where the AIO-AFSAT boundary was (indicated by an arrow in the plot labeled AIO REV). It seems unlikely, therefore, that the disagreement is due to movement of a boundary.

It is evident, however, that the character of the auroral ionosphere changed in the time between the pass shown in the plot labeled REV-1 and the pass of interest. The background density level poleward of the location of the AIO-AFSAT boundary is higher than it was in the previous pass and contains larger irregularity structures. The C_kL estimates calculated from the SSIES data show a general decrease through this region, but it is not enough to match that seen in the AIO-AFSAT data (as seen in the lower plot in Figure 6).

At this point it is not clear whether there is an as-yet unresolved problem with these data sets, or if this may be an indication that there are times when the irregularity strength observed at the DMSP satellite is not representative of the strength of irregularities throughout the layer (i.e., near the F2 peak). Now that there is a case where the *in-situ* data characterized the beacon data well (from the 1988 campaign) and one where it does not (the current case), it is imperative that the additional days' data from this campaign be processed and analyzed to try to determine wherein the problem lies.

There is one final observation to be made from this data set. The middle plot in Figure 6 shows the phase spectral slope parameter, p, from the AIO-AFSAT phase spectra, calculated by adding one to the slope of the SSIES *in-situ* spectrum (q), and from the WBMOD model. With the exception of the final point, all of the slopes calculated from the *in-situ* data are steeper than both the WBMOD and AIO-AFSAT slopes. If nothing else, this indicates that we may not be able to use the slopes calculated from the *in-situ* data to characterize the entire layer even if we find how to scale the C_k data correctly. This is not as critical a problem as the C_k-scaling since

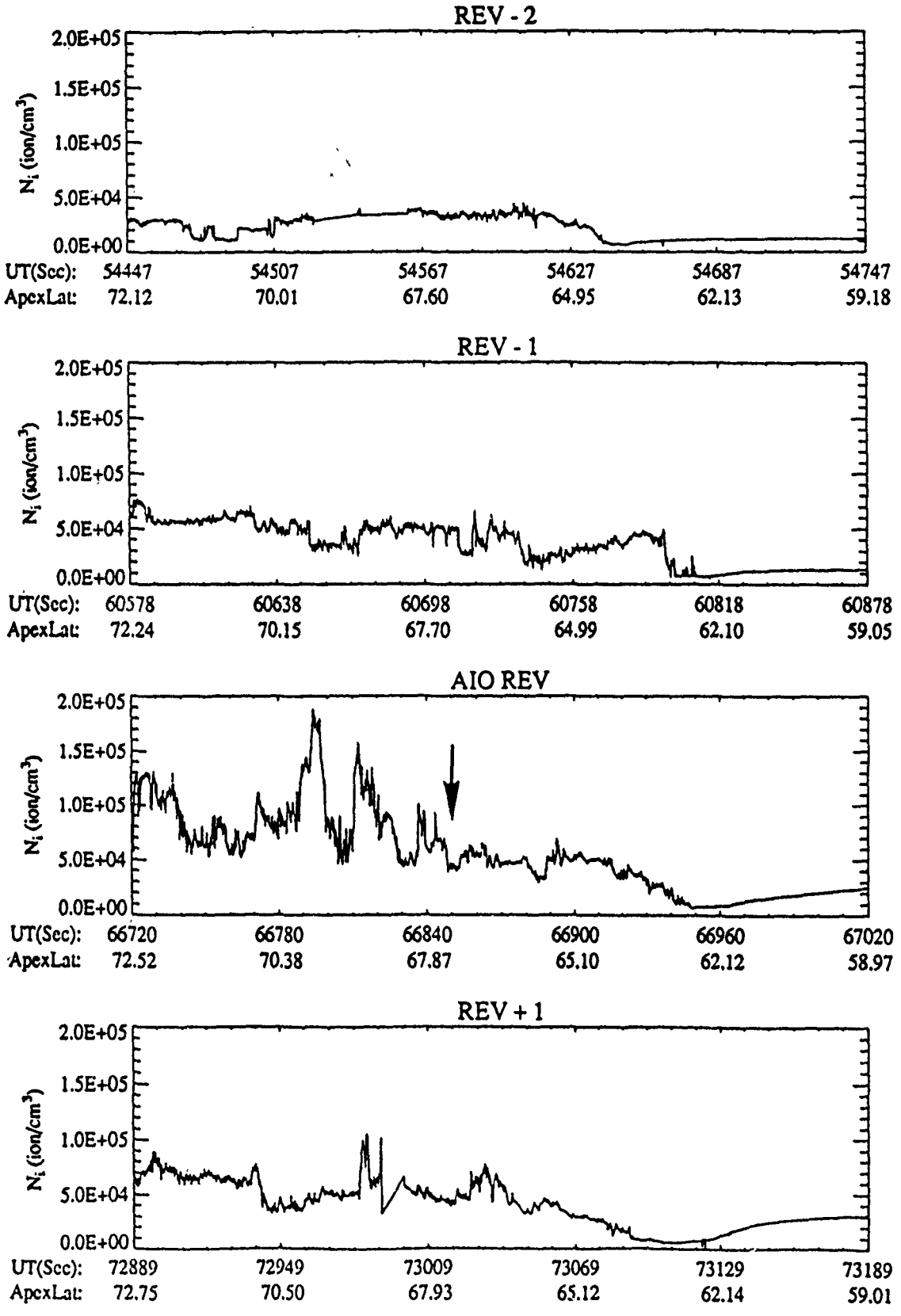

Figure 7. The variation of total ion density through the northern-hemisphere, pre-midnight auroral ionosphere for four sequential DMSP passes. The arrow in the AIO-REV plot shows the location of the AIO-AFSATCOM scintillation "boundary."

the slope values vary over a much smaller range, but it does provide an indication that the character of the irregularity spectrum is not constant throughout the layer.

3. Conclusion

Data from the first of five data sets collected in the January 1990 SSIES/AIO/EISCAT data-collection campaign have been analyzed. The results of the analysis are not as promising as those obtained in the assessment study from the January 1988 campaign, and it is not yet clear whether the problem is with the *in-situ* C_k estimate or with the procedure used to scale C_k to C_kL. This issue will be addressed in more detail when the EISCAT profile data become available.

REFERENCES.

[1] Secan, J. A., *An Assessment of the Application of In Situ Ion-Density Data From DMSP to Modeling of Transionospheric Scintillation, Final Report, GL-TR-90-0093,* Geophysics Laboratory (AFSC), Hanscom AFB, MA, 1990, ADA224392.

[2] Rino, C. L., "A power law phase screen model for ionospheric scintillations, 1. Weak scatter," *Radio Sci., 14,* 1135-1145, 1979.

[3] Fremouw, E. J. and Lansinger, J. M., *A Computer Model for High-Latitude Phase Scintillation Based on WIDEBAND Satellite data From Poker Flat,* DNA Report 5685F, Defense Nuclear Agency, Washington, DC, February 1981.

[4] Secan, J. A., E. J. Fremouw, and R. E. Robins, "A review of recent improvements to the WBMOD ionospheric scintillation model," in *The Effect of the Ionosphere on Communications, Navigation, and Surveillance Systems,* edited by J. Goodman, Naval Research Laboratory, Washington, DC, 607-616, 1987.

Appendix A: Summary Data Plots for the 1990 SSIES/AIO Campaign

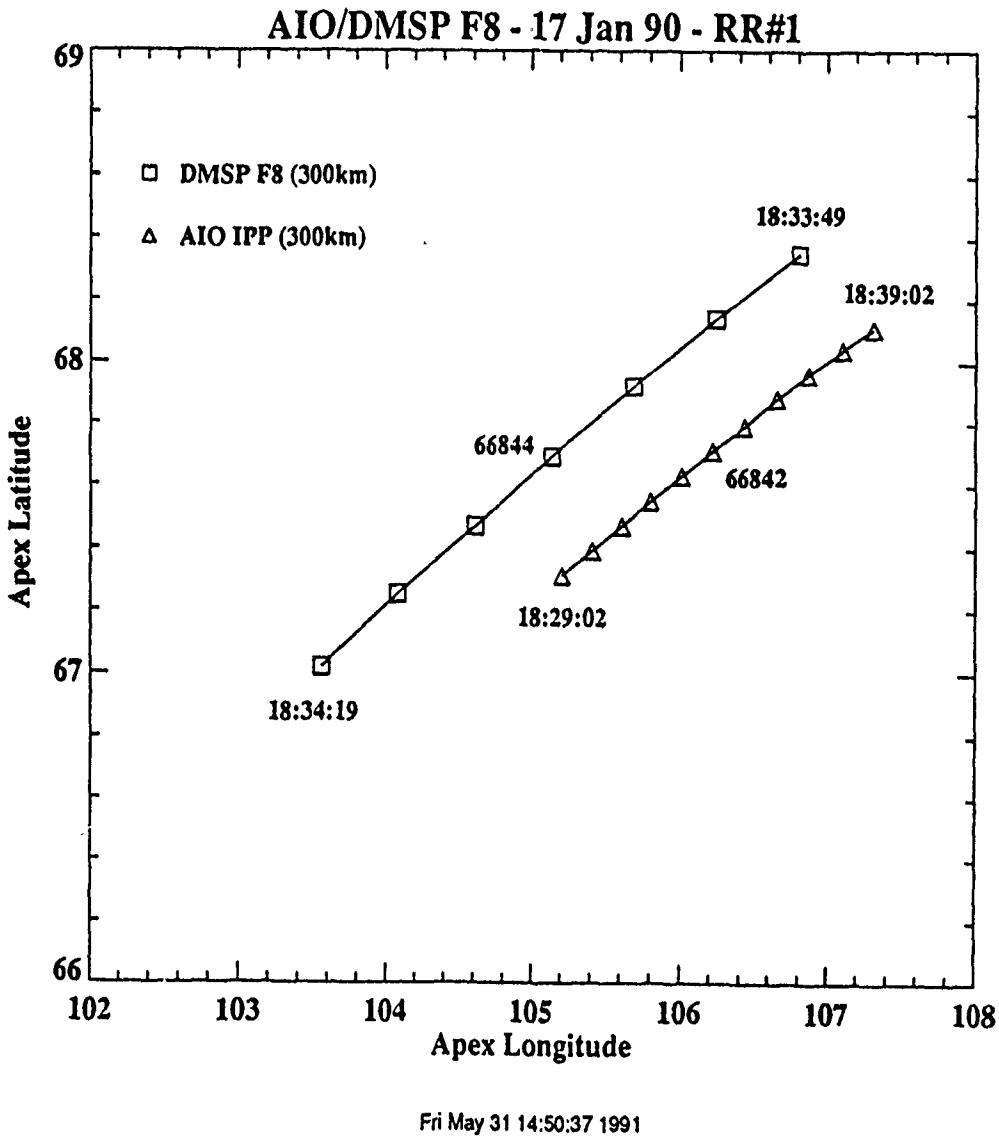

Figure A-1. Geometry of the SSIES/AIO experiment for 17 January 1990. The locations of the AIO-AFSATCOM 300-km ionospheric penetration point (IPP) and the SSIES 300-km field-line footprint are shown. The time/location of closest approach is indicated by time tags near the center of each location trace.

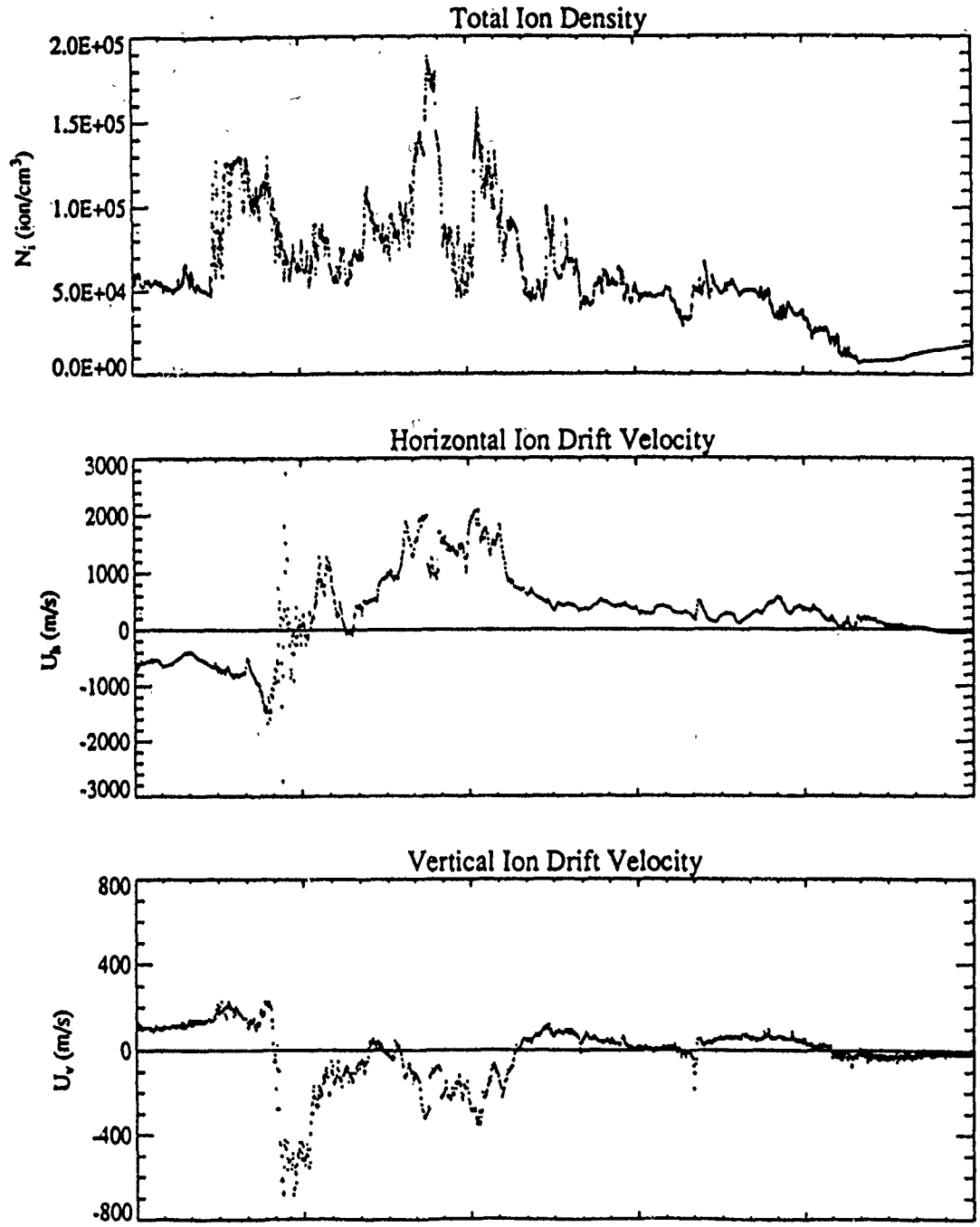

Figure A-2. The variation of the total ion density from the SSIES SM sensor (top plot), the horizontal cross-track ion drift velocity from the DM sensor (U_h) (middle plot), and the vertical cross-track velocity from the DM sensor (U_v) (bottom plot) with time and location along the DMSP orbit for 17 January 1990. (Note: A positive value for U_h corresponds to flow in the sunward direction.)

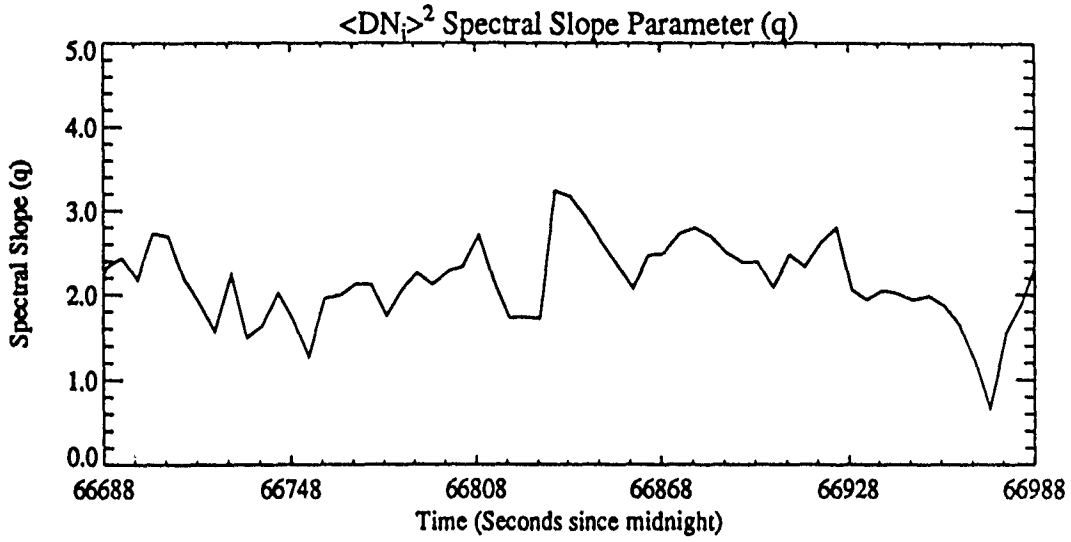

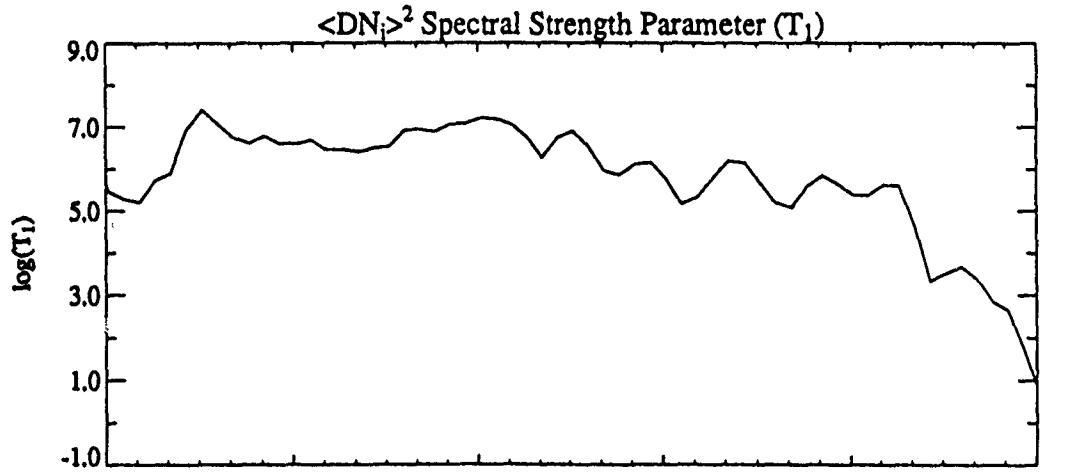

UT(Sec):	66688	66748	66808	66868	66928	66988
GeogLat:	77.66	75.03	72.14	69.09	65.96	62.78
GeogLon:	38.58	29.09	22.42	17.52	13.77	10.79
Alt:	848.26	848.05	847.79	847.49	847.14	846.77
ApexLat:	73.47	71.57	69.25	66.61	63.73	60.67
ApexLon:	127.90	117.59	109.30	102.66	97.31	92.92
ApexLT:	22.33	21.66	21.13	20.70	20.36	20.09

Time / 300 km Trace Position

Fri May 24 10:35:36 1991

Figure A-3. The slope (q) (top plot) and strength (T_1) (bottom plot) of the *in-situ* spectrum derived from the (detrended) SSIES SM density data plotted for the same time period covered in Figure A-2.

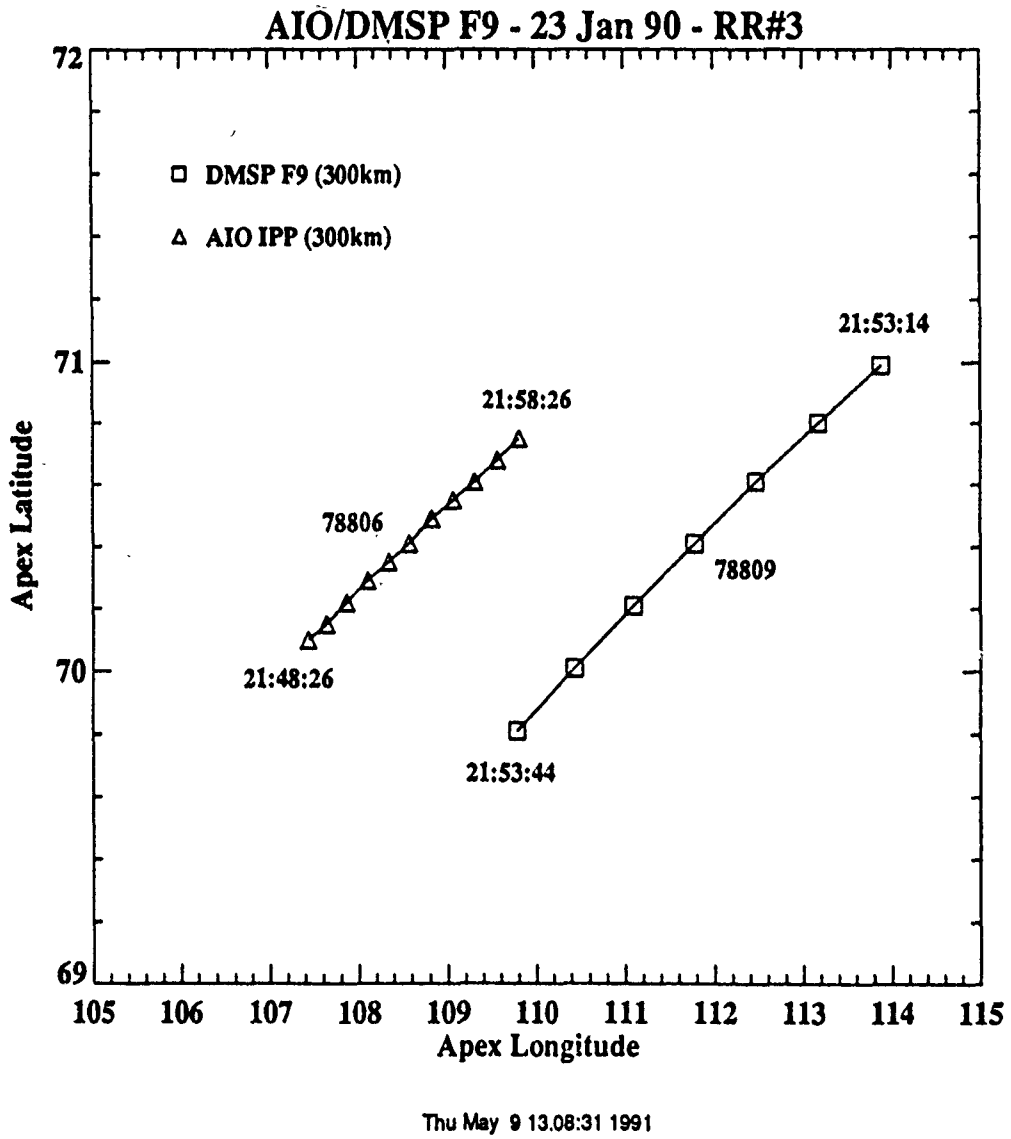

Figure A-4. Geometry of the SSIES/AIO experiment for 23 January 1990. The locations of the AIO-AFSATCOM 300-km ionospheric penetration point (IPP) and the SSIES 300-km field-line footprint are shown. The time/location of closest approach is indicated by time tags near the center of each location trace.

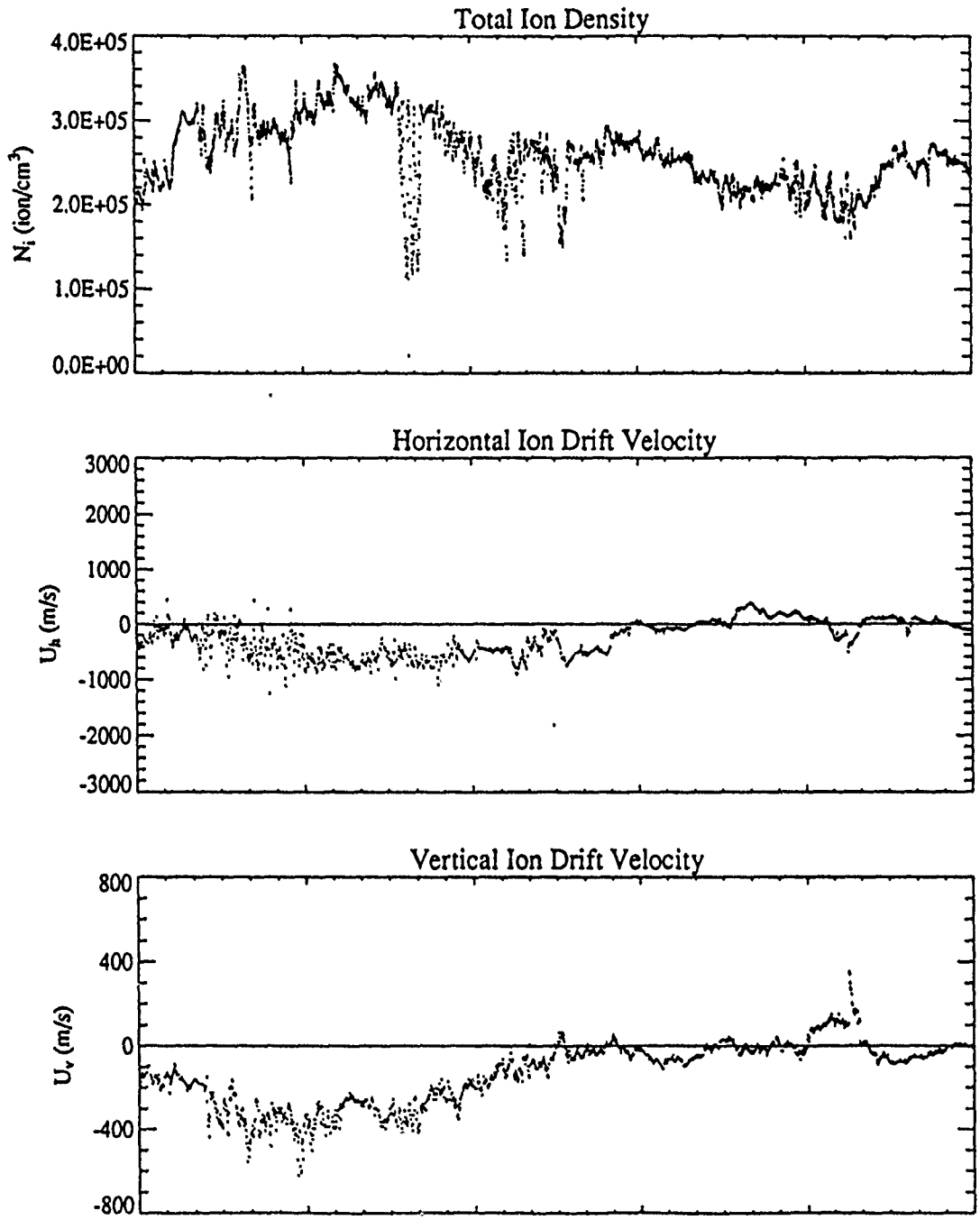

UT(Sec):	78659	78719	78779	78839	78899	78959
GeogLat:	79.82	77.57	74.89	71.96	68.89	65.74
GeogLon:	49.95	36.47	27.27	20.81	16.06	12.43
Alt:	836.89	836.90	836.81	836.61	836.31	835.92
ApexLat:	74.86	73.49	71.55	69.18	66.51	63.60
ApexLon:	138.72	126.33	116.11	107.91	101.37	96.10
ApexLT:	2.27	1.46	0.80	0.27	23.85	23.51

Time / 300 km Trace Position

Figure A-5. The variation of the total ion density from the SSIES SM sensor (top plot), the horizontal cross-track ion drift velocity from the DM sensor (U_h) (middle plot), and the vertical cross-track velocity from the DM sensor (U_v) (bottom plot) with time and location along the DMSP orbit for 23 January 1990. (Note: A positive value for U_h corresponds to flow in the sunward direction.)

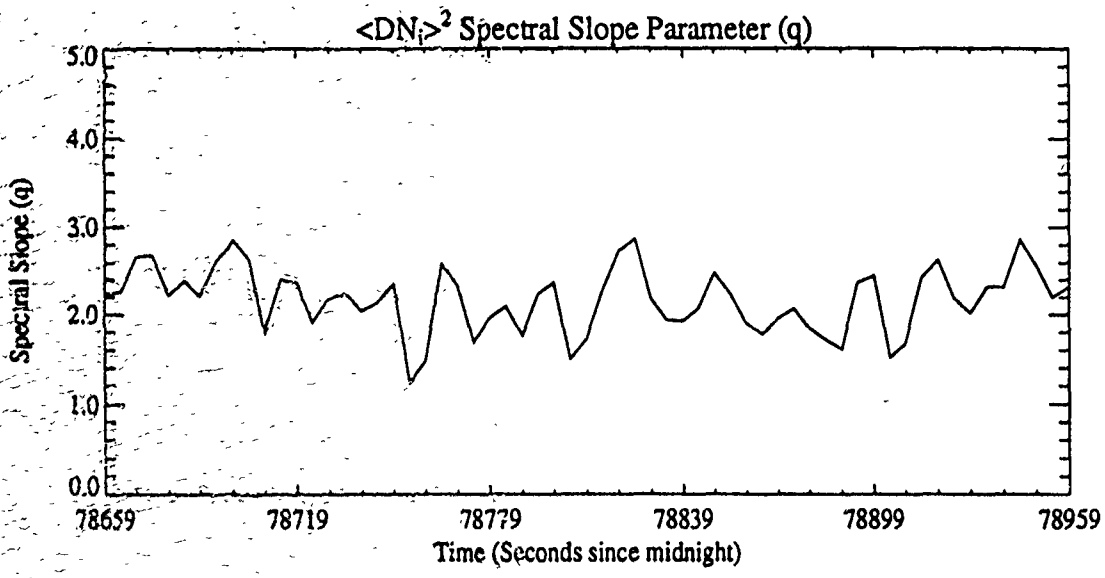

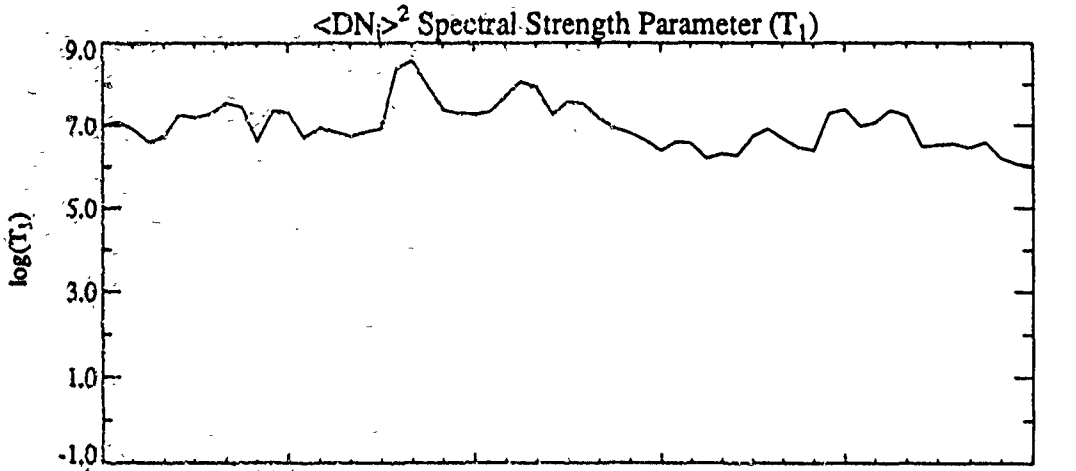

UT(Sec):	78659	78719	78779	78839	78899	78959
GeogLat:	79.82	77.57	74.89	71.96	68.89	65.74
GeogLon:	49.95	36.47	27.27	20.81	16.06	12.43
Alt:	836.89	836.90	836.81	836.61	836.31	835.92
ApexLat:	74.86	73.49	71.55	69.18	66.51	63.60
ApexLon:	138.72	126.33	116.11	107.91	101.37	96.10
ApexLT:	2.27	1.46	0.80	0.27	23.85	23.51

Time / 300 km Trace Position

Figure A-6. The slope (q) (top plot) and strength (T_1) (bottom plot) of the *in-situ* spectrum derived from the (detrended) SSIES SM density data plotted for the same time period covered in Figure A-5.

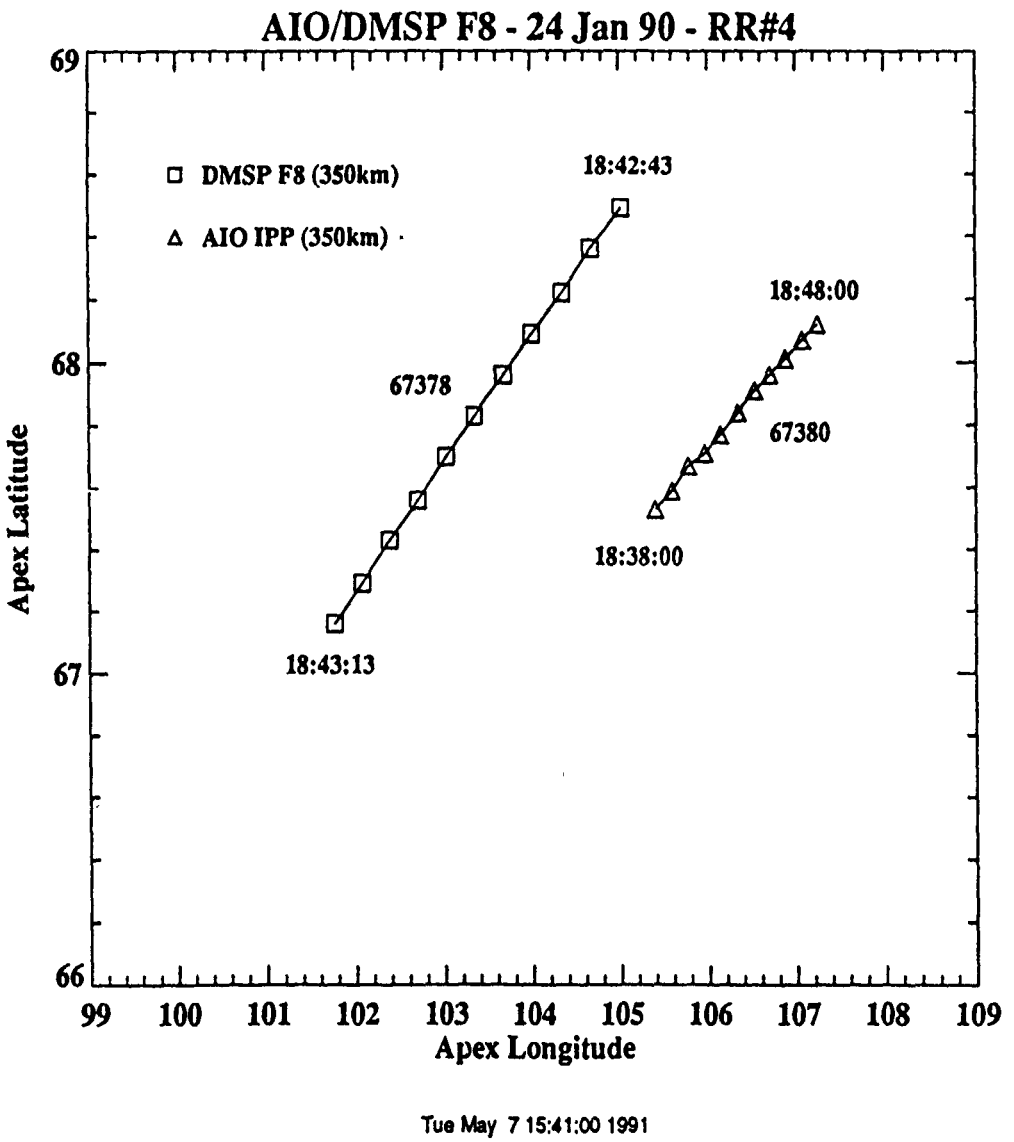

Figure A-7. Geometry of the SSIES/AIO experiment for 24 January 1990. The locations of the AIO-AFSATCOM 300-km ionospheric penetration point (IPP) and the SSIES 300-km field-line footprint are shown. The time/location of closest approach is indicated by time tags near the center of each location trace.

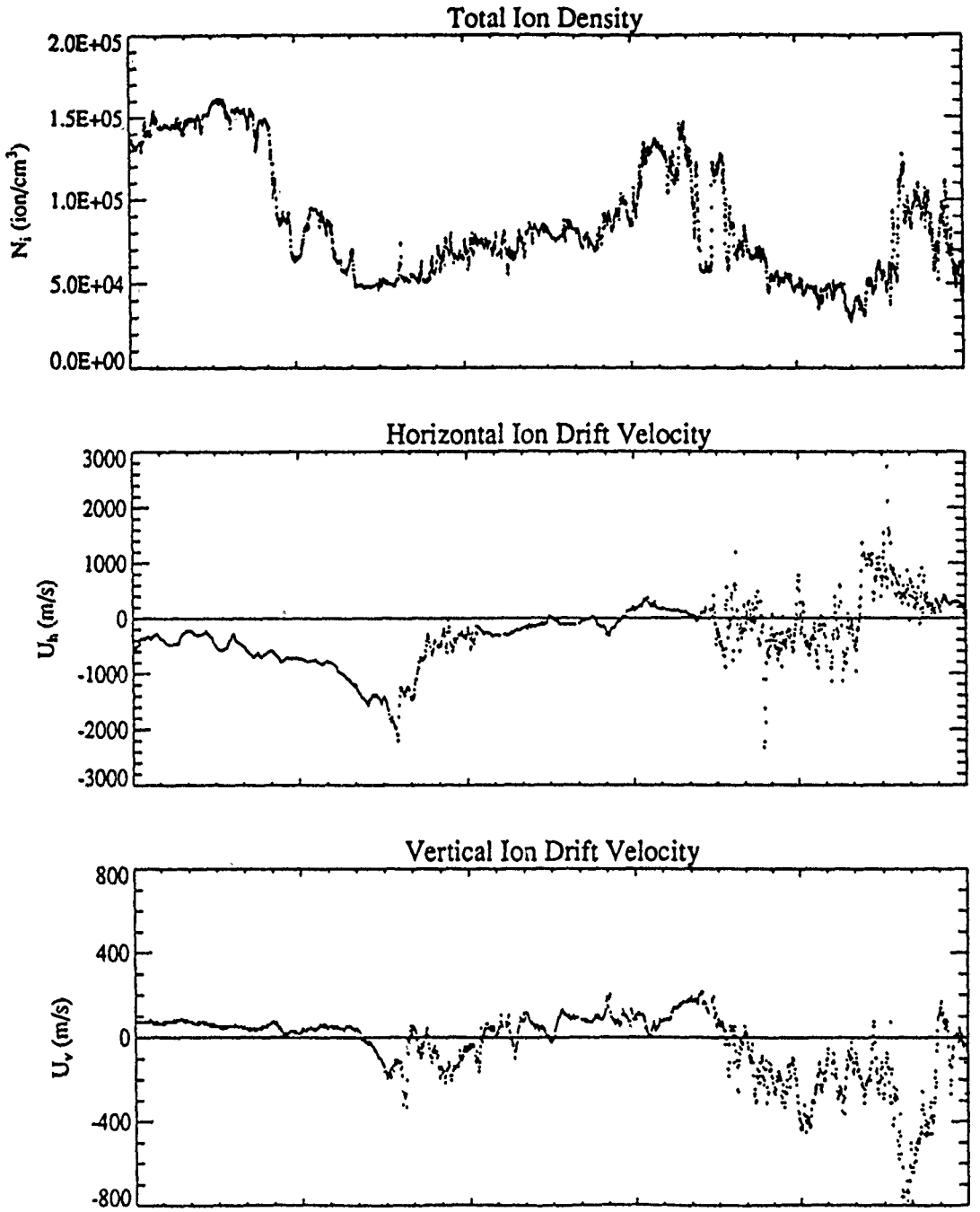

UT(Sec):	67228	67288	67348	67408	67468	67528
GeogLat:	77.39	74.72	71.81	68.75	65.62	62.44
GeogLon:	35.06	25.96	19.52	14.78	11.14	8.23
Alt:	849.51	849.52	849.47	849.37	849.23	849.05
ApexLat:	73.41	71.48	69.13	66.47	63.58	60.50
ApexLon:	125.10	114.95	106.80	100.27	95.01	90.69
ApexLT:	22.30	21.64	21.11	20.69	20.36	20.09

Time / 300 km Trace Position

Figure A-8. The variation of the total ion density from the SSIES SM sensor (top plot), the horizontal cross-track ion drift velocity from the DM sensor (U_h) (middle plot), and the vertical cross-track velocity from the DM sensor (U_v) (bottom plot) with time and location along the DMSP orbit for 24 January 1990. (Note: A positive value for U_h corresponds to flow in the sunward direction.)

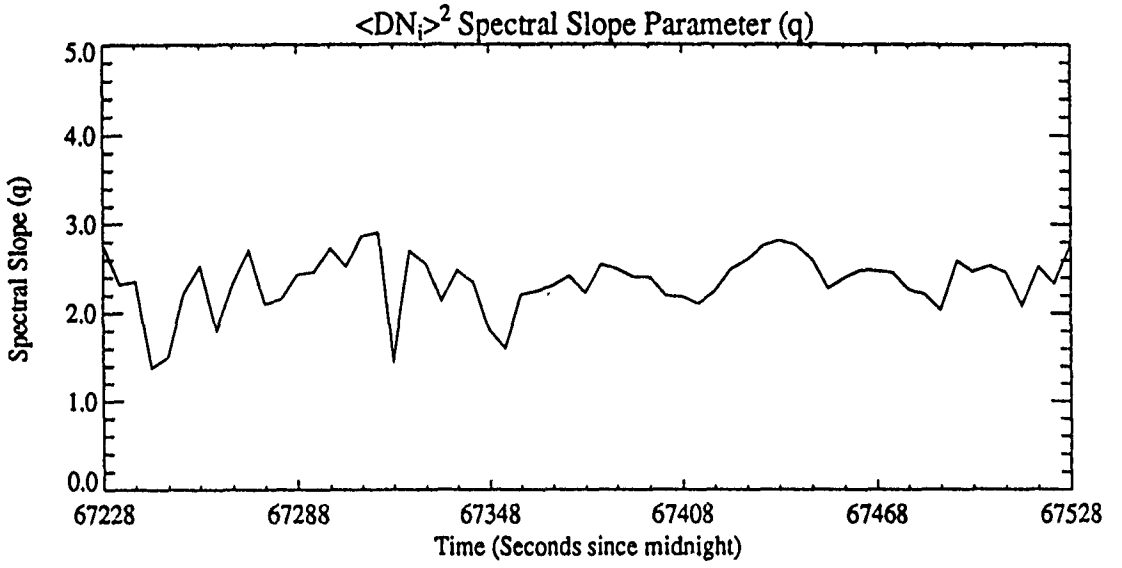

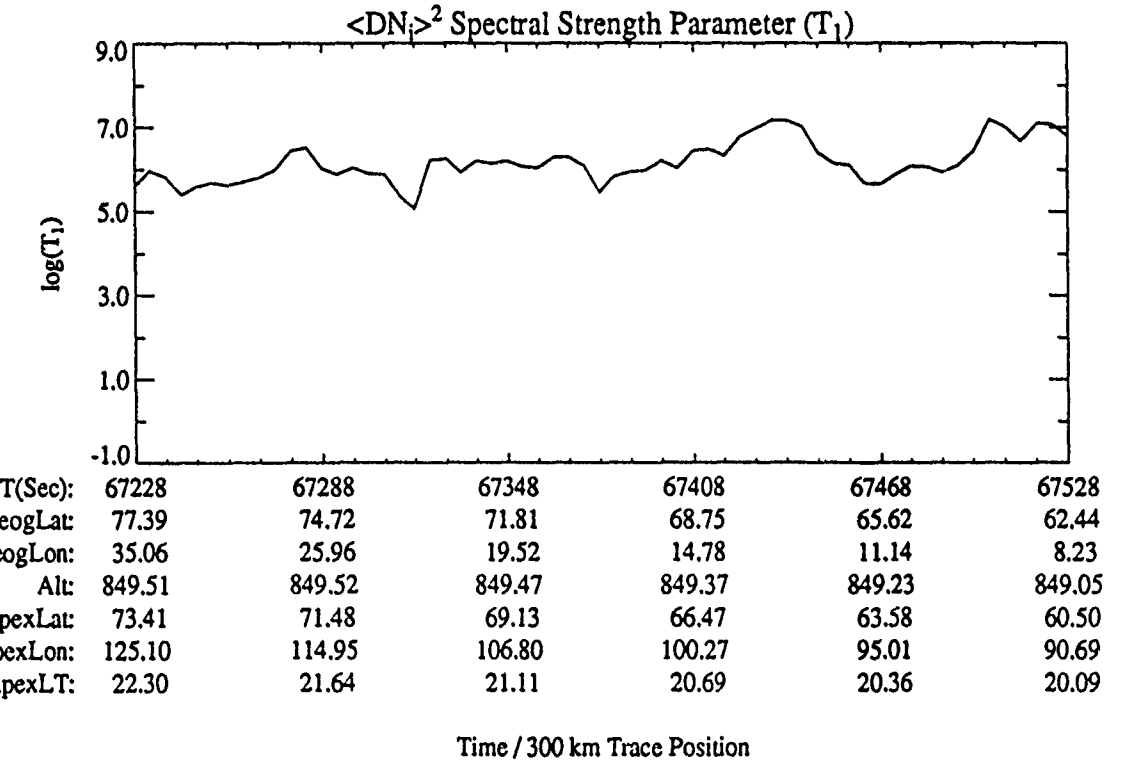

Figure A-9. The slope (q) (top plot) and strength (T_1) (bottom plot) of the *in-situ* spectrum derived from the (detrended) SSIES SM density data plotted for the same time period covered in Figure A-8.

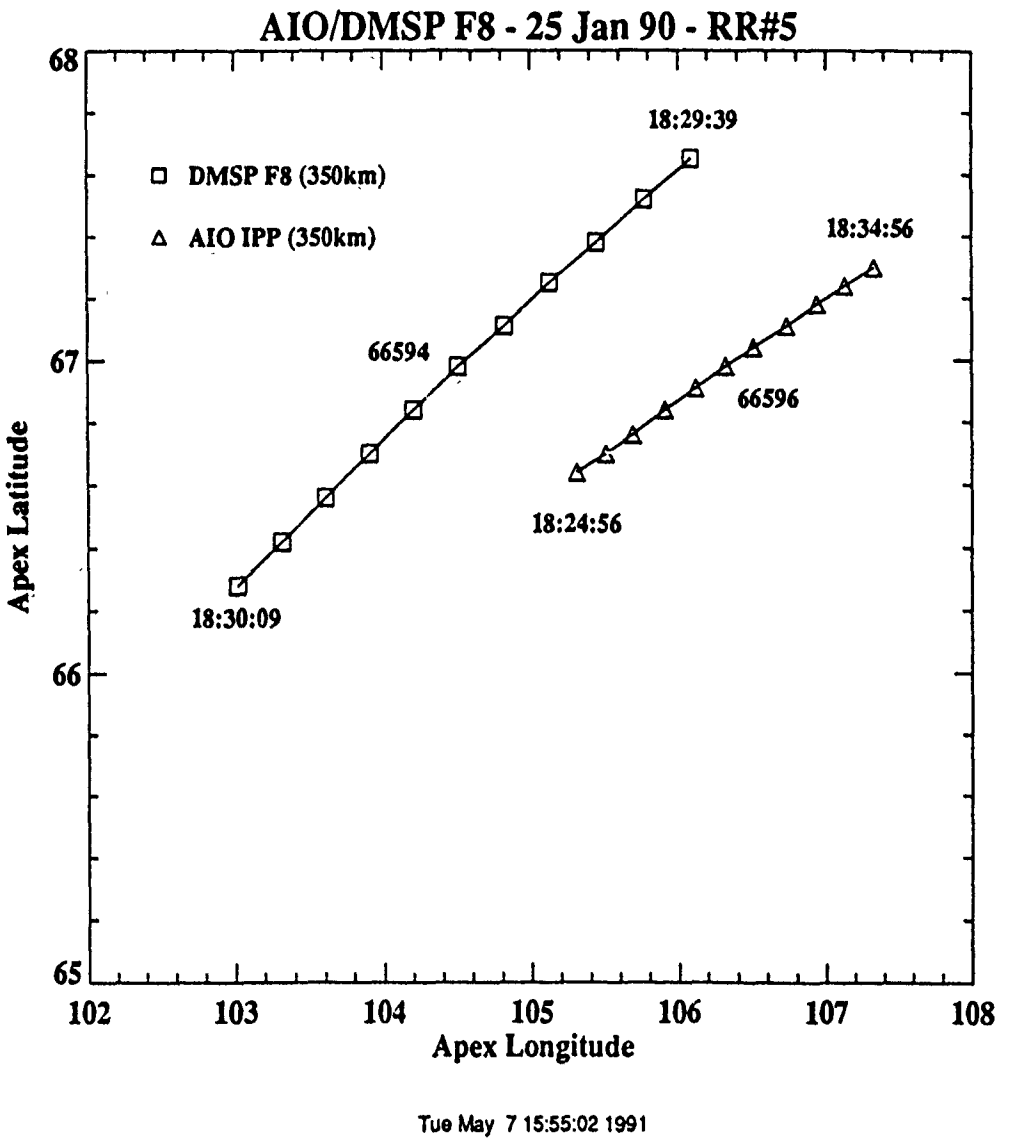

Figure A-10. Geometry of the SSIES/AIO experiment for 25 January 1990. The locations of the AIO-AFSATCOM 300-km ionospheric penetration point (IPP) and the SSIES 300-km field-line footprint are shown. The time/location of closest approach is indicated by time tags near the center of each location trace.

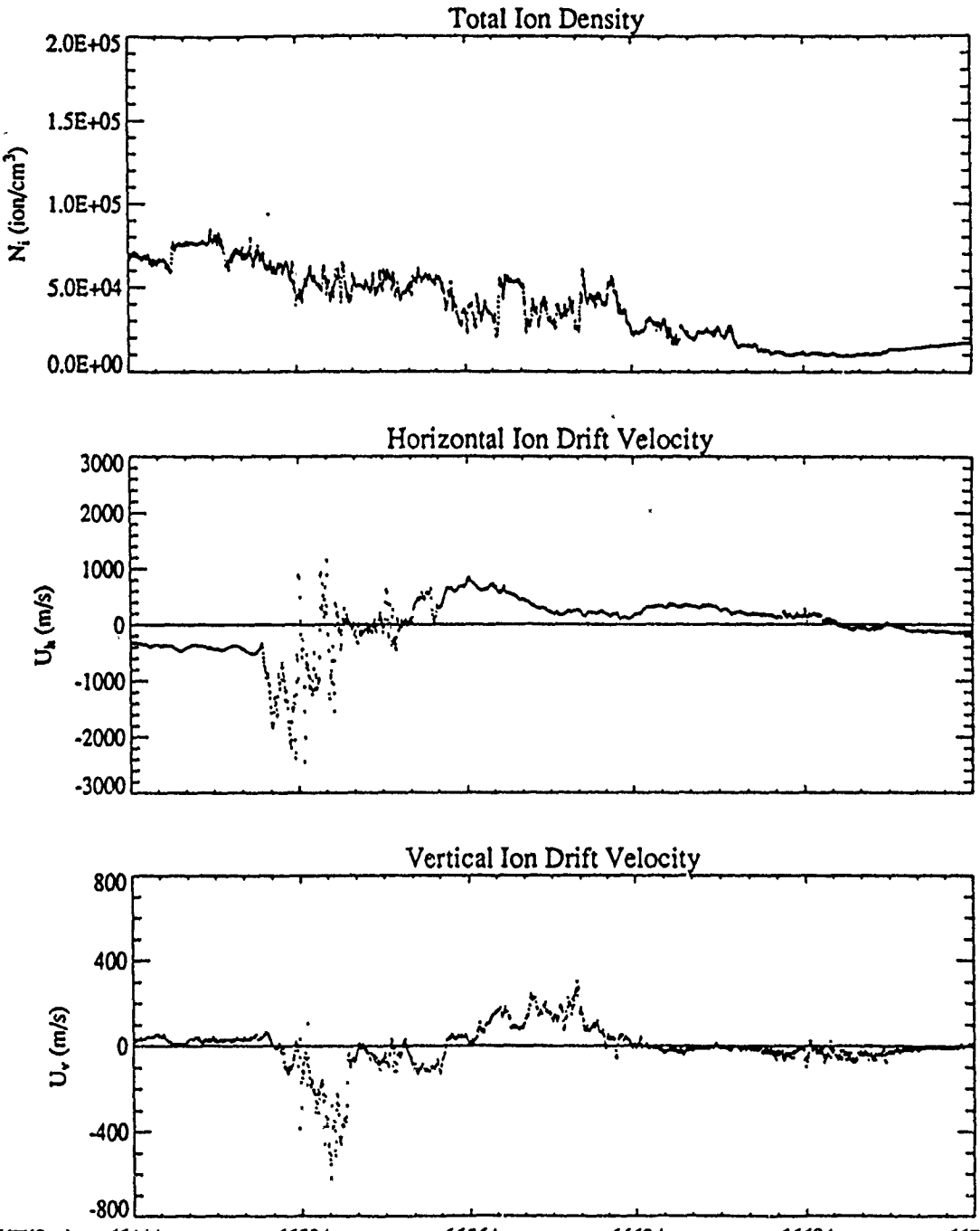

Figure A-11. The variation of the total ion density from the SSIES SM sensor (top plot), the horizontal cross-track ion drift velocity from the DM sensor (U_h) (middle plot), and the vertical cross-track velocity from the DM sensor (U_v) (bottom plot) with time and location along the DMSP orbit for 25 January 1990. (Note: A positive value for U_h corresponds to flow in the sunward direction.)

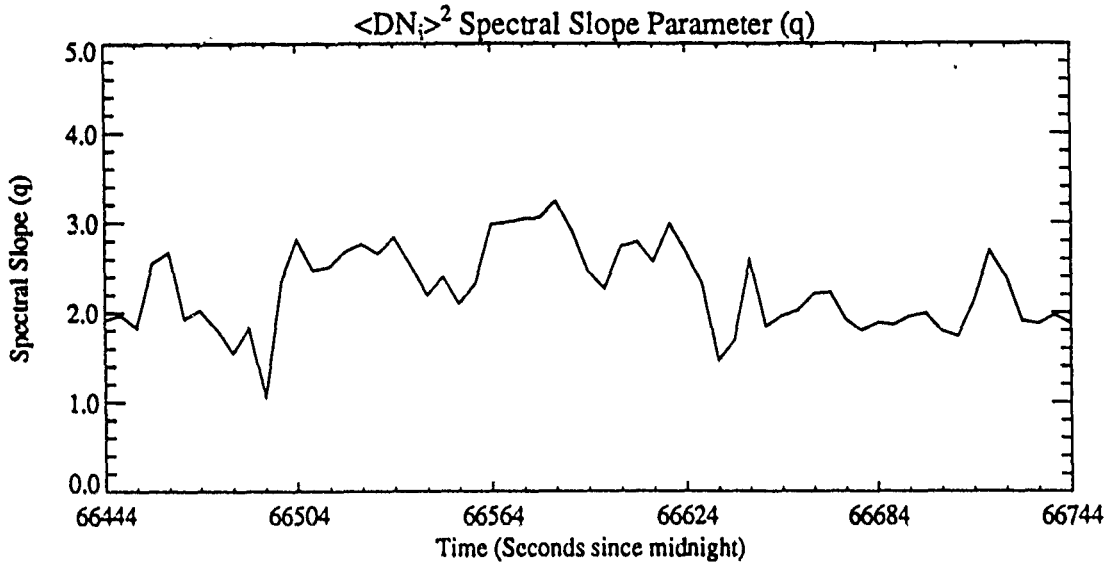

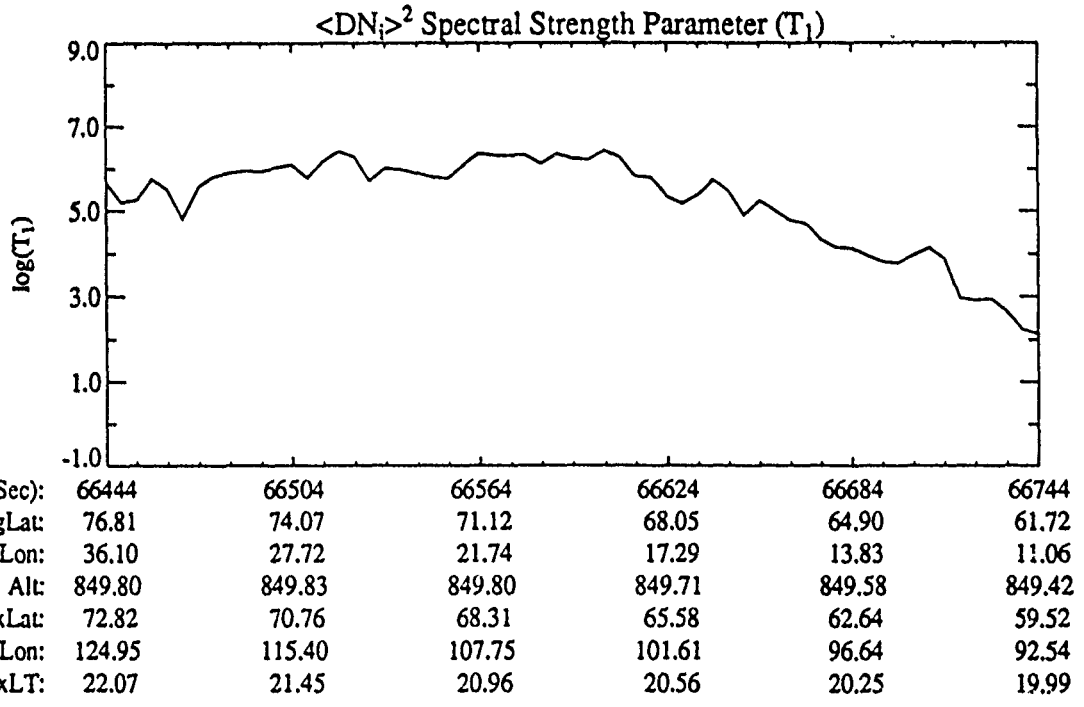

Figure A-12. The slope (q) (top plot) and strength (T_1) (bottom plot) of the *in-situ* spectrum derived from the (detrended) SSIES SM density data plotted for the same time period covered in Figure A-11.

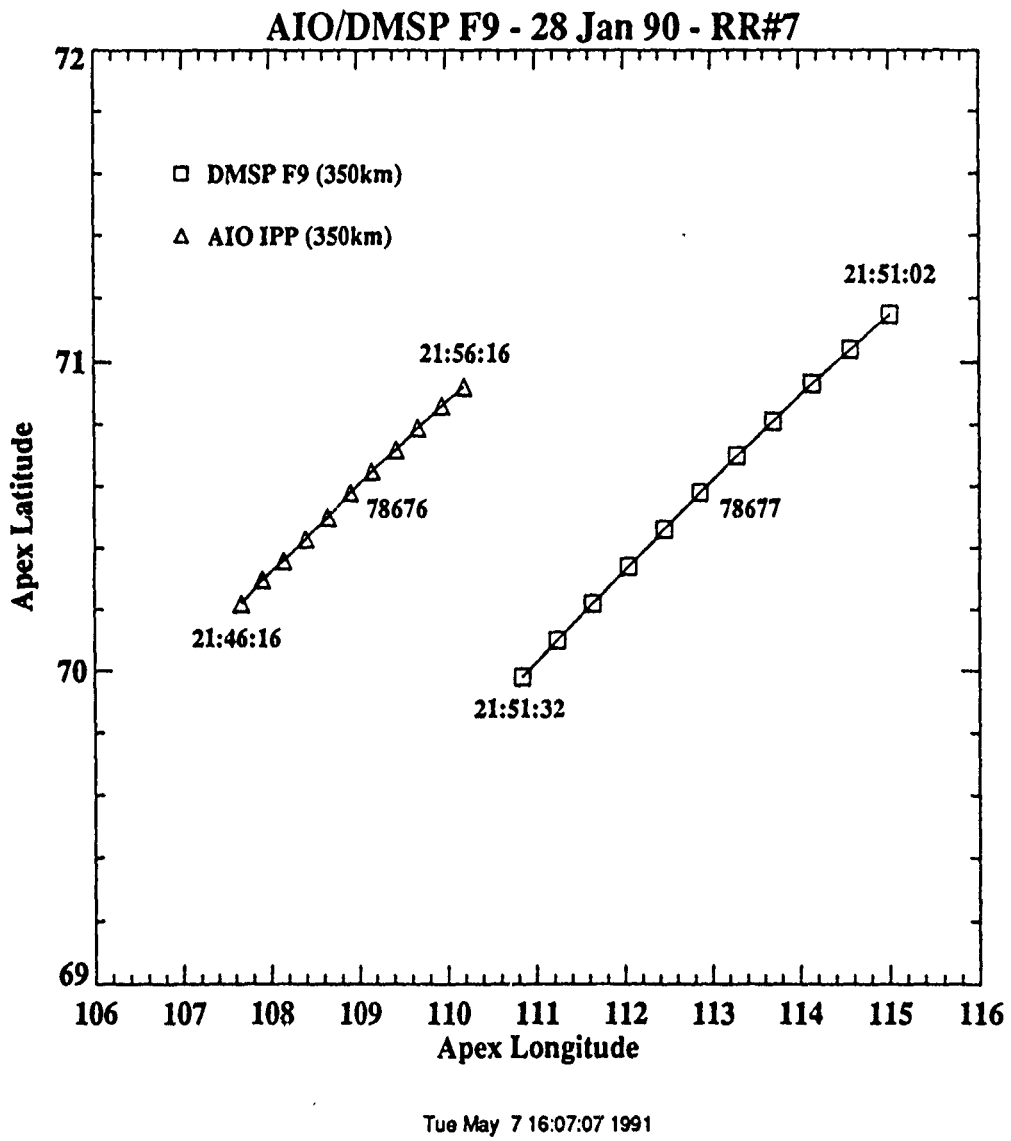

Figure A-13. Geometry of the SSIES/AIO experiment for 28 January 1990. The locations of the AIO-AFSATCOM 300-km ionospheric penetration point (IPP) and the SSIES 300-km field-line footprint are shown. The time/location of closest approach is indicated by time tags near the center of each location trace.

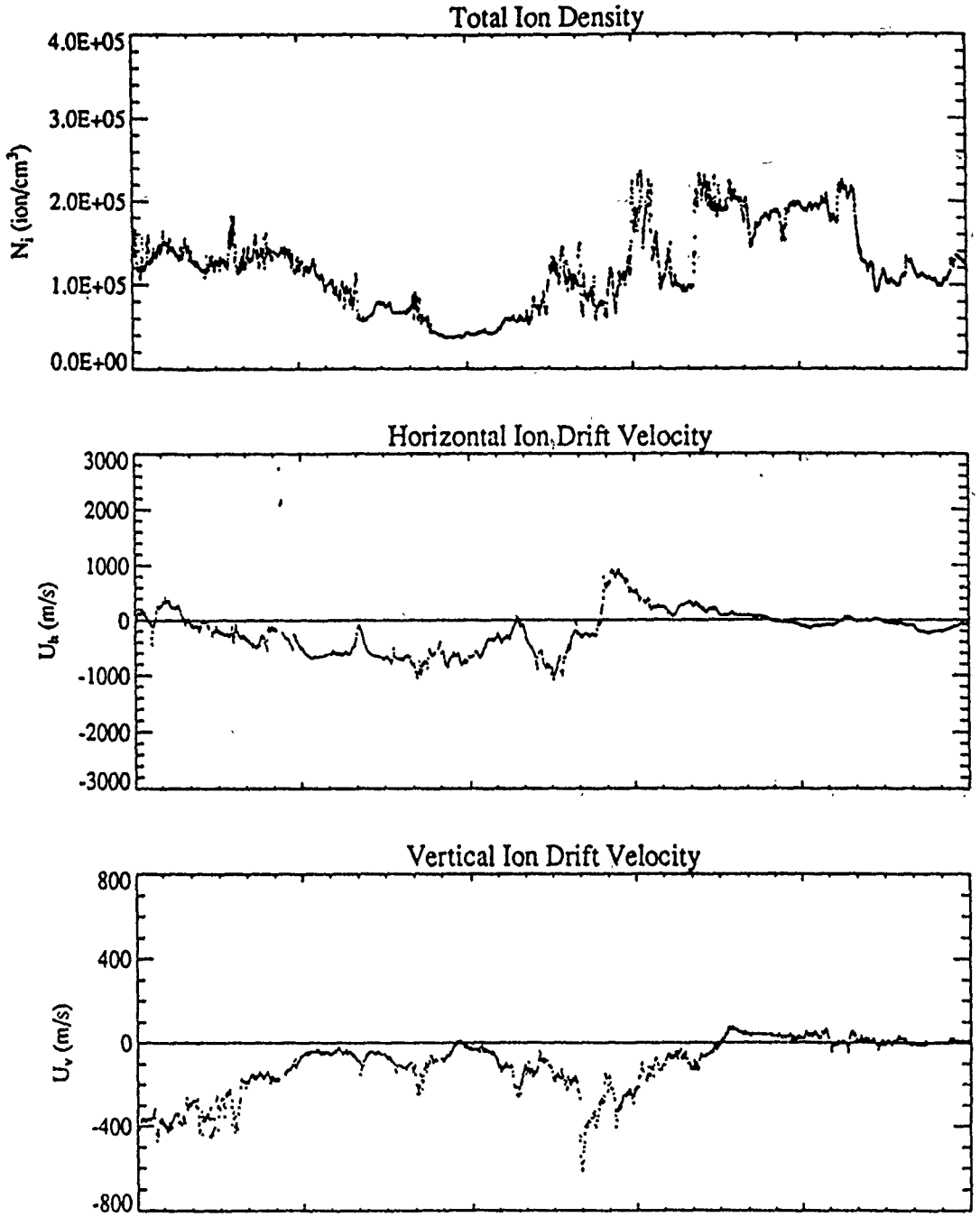

UT(Sec):	78527	78587	78647	78707	78767	78827
GeogLat:	79.98	77.78	75.13	72.22	69.16	66.01
GeogLon:	51.88	37.96	28.46	21.81	16.95	13.23
Alt:	837.85	837.83	837.69	837.45	837.10	836.66
ApexLat:	74.92	73.61	71.70	69.36	66.71	63.82
ApexLon:	140.20	127.66	117.27	108.94	102.28	96.93
ApexLT:	2.34	1.52	0.84	0.30	23.87	23.53

Time / 300 km Trace Position

Figure A-14. The variation of the total ion density from the SSIES SM sensor (top plot), the horizontal cross-track ion drift velocity from the DM sensor (U_h) (middle plot), and the vertical cross-track velocity from the DM sensor (U_v) (bottom plot) with time and location along the DMSP orbit for 28 January 1990. (Note: A positive value for U_h corresponds to flow in the sunward direction.)

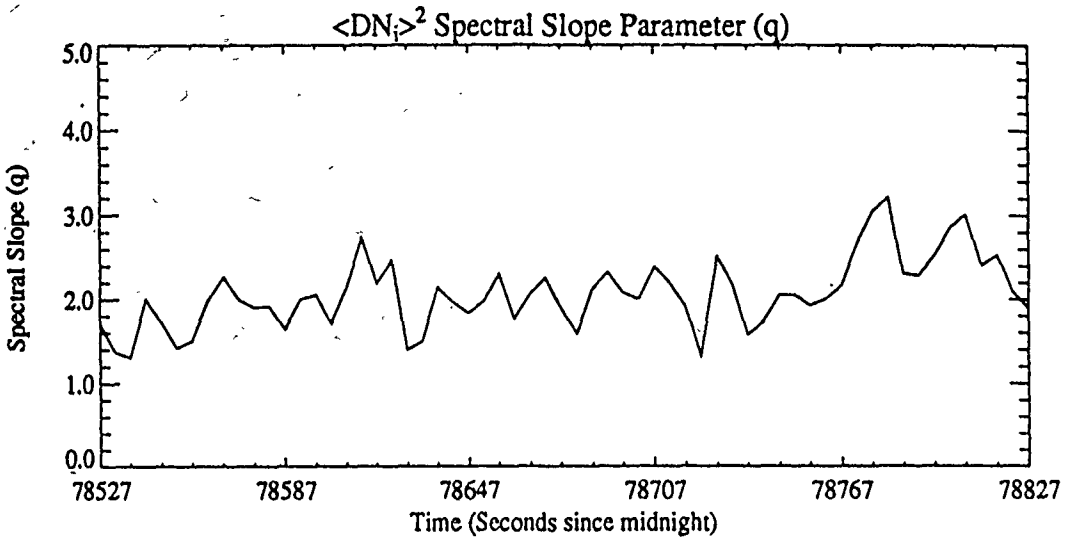

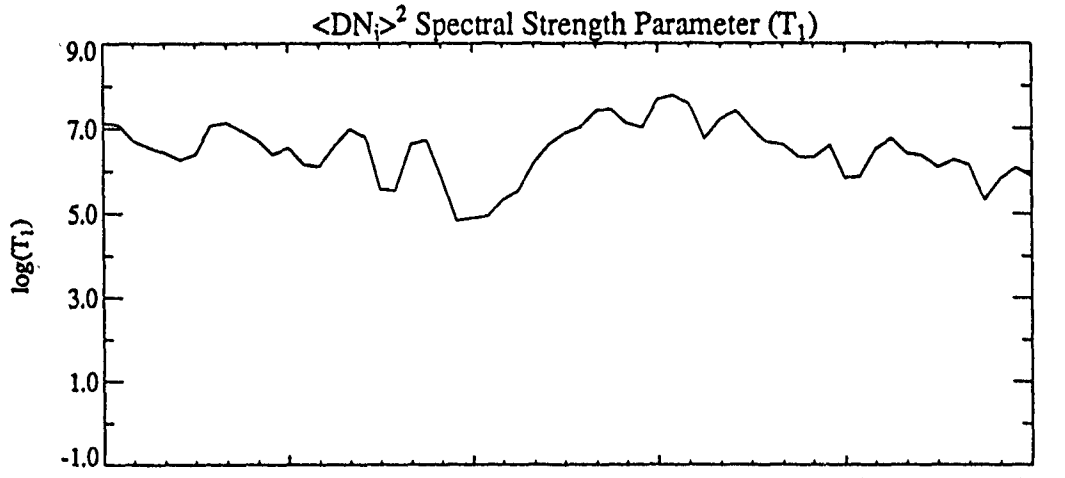

UT(Sec):	78527	78587	78647	78707	78767	78827
GeogLat:	79.98	77.78	75.13	72.22	69.16	66.01
GeogLon:	51.88	37.96	28.46	21.81	16.95	13.23
Alt:	837.85	837.83	837.69	837.45	837.10	836.66
ApexLat:	74.92	73.61	71.70	69.36	66.71	63.82
ApexLon:	140.20	127.66	117.27	108.94	102.28	96.93
ApexLT:	2.34	1.52	0.84	0.30	23.87	23.53

Time / 300 km Trace Position

Figure A-15. The slope (q) (top plot) and strength (T_1) (bottom plot) of the *in-situ* spectrum derived from the (detrended) SSIES SM density data plotted for the same time period covered in Figure A-14.

Appendix B: Data and PDS Plots for 17 January 1990

This appendix contains plots of the detrended SSIES density data with corresponding PDS and the detrended AIO-AFSAT phase data with corresponding PDS for each of the nine data segments identified in Table 3 and on Figures 1 and 4. Each plot is labeled with the segment number in the upper left corner of the detrended-data plot at the top of the figure.

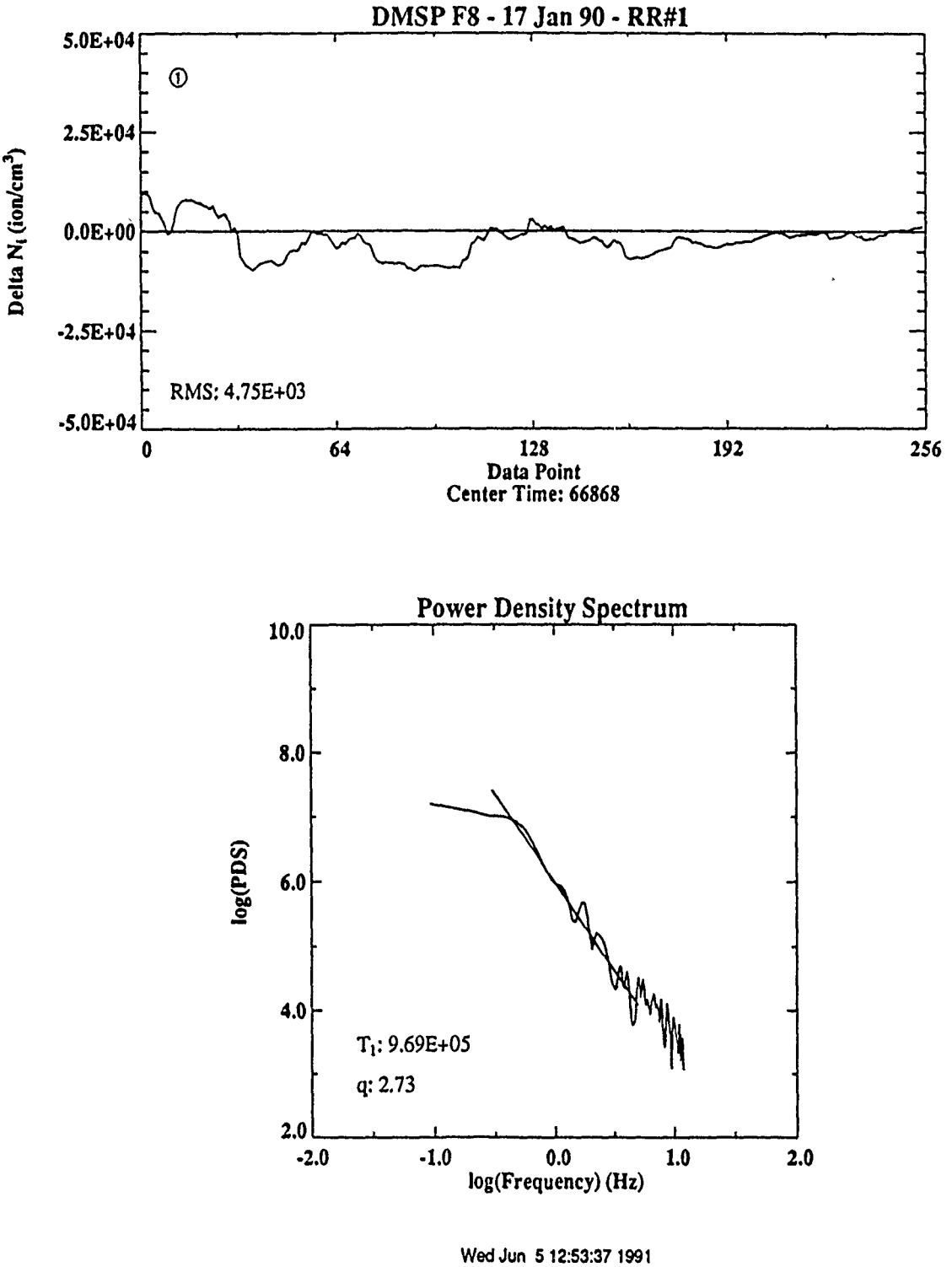

Figure B-1. Detrended total ion density from the DMSP SSIES SM sensor (top plot) and the PDS generated from this data sample (lower plot) for data point no. 1 as identified in Table 3. The straight line plotted over the PDS is the power-law fit used to estimate T_1 and q.

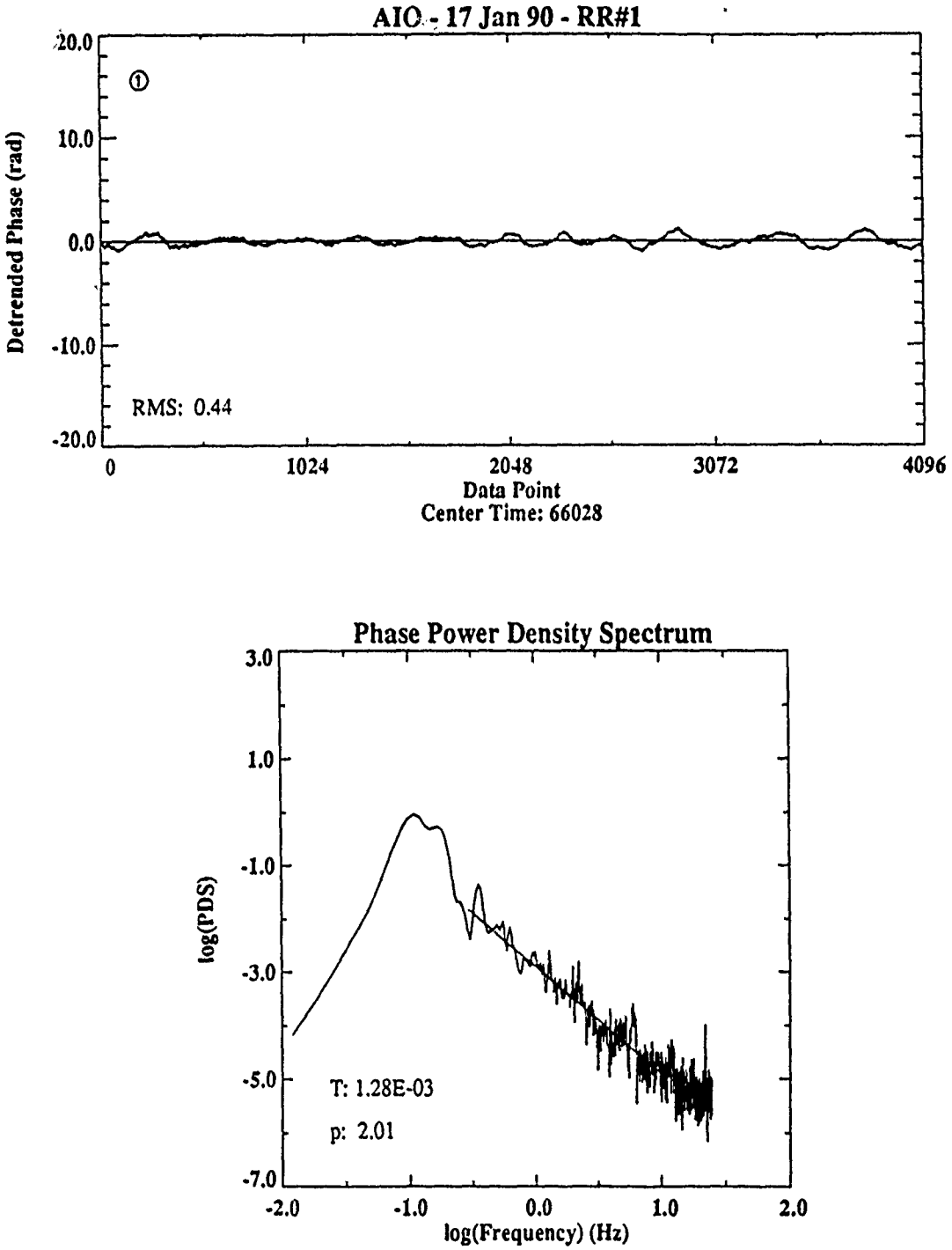

Figure B-2. Detrended phase from the AIO-AFSATCOM link (top plot) and the PDS generated from this data sample (lower plot) for data point no. 1 as identified in Table 3. The straight line plotted over the PDS is the power-law fit used to estimate T and p.

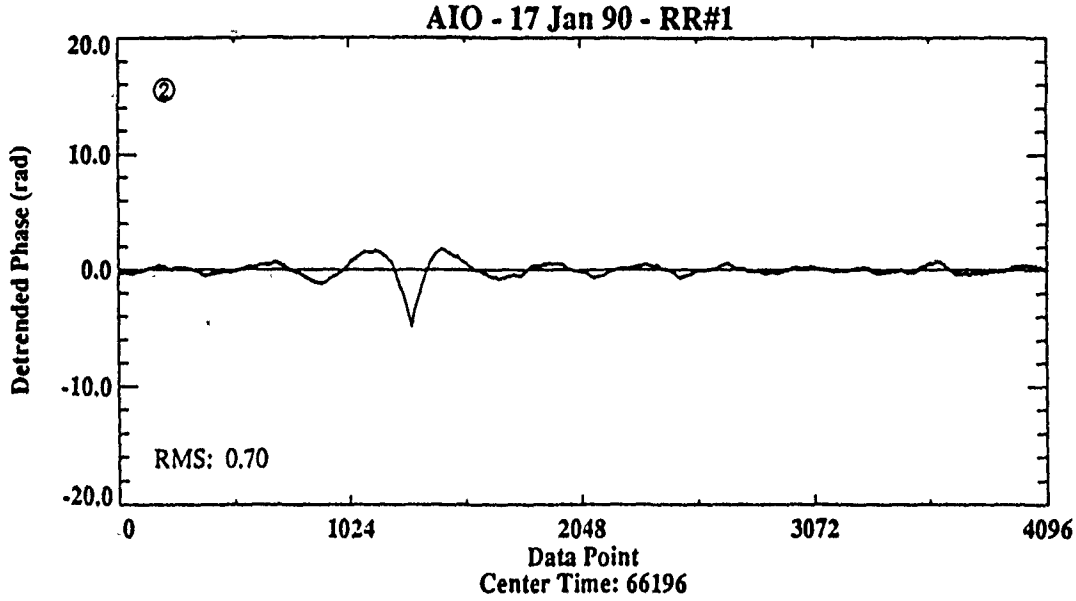

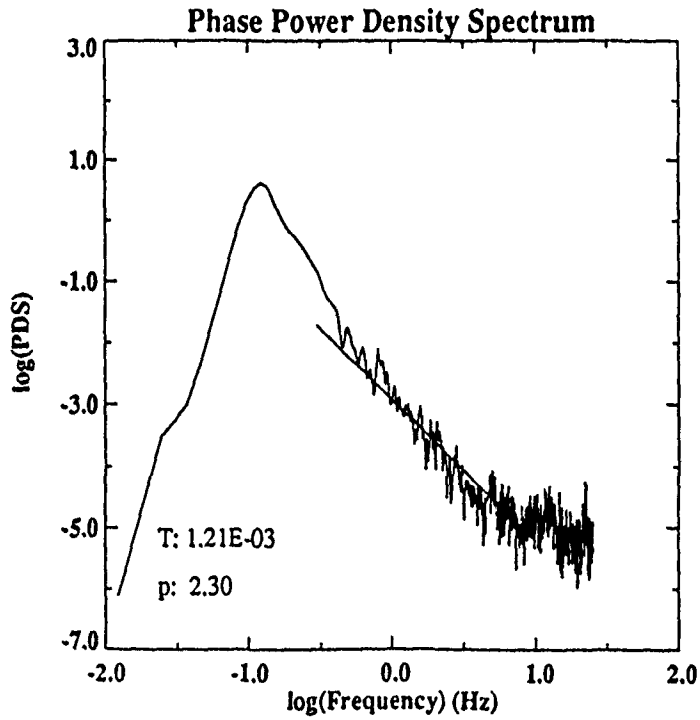

Figure B-4. The same as plot B-2 (AIO-AFSATCOM data) for data point no. 2.

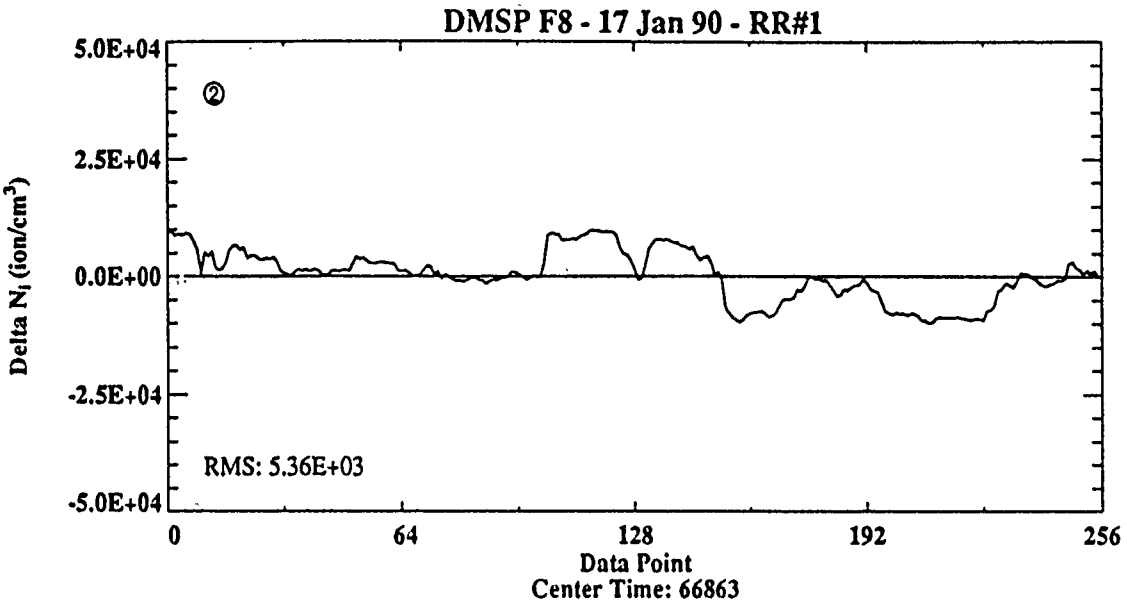

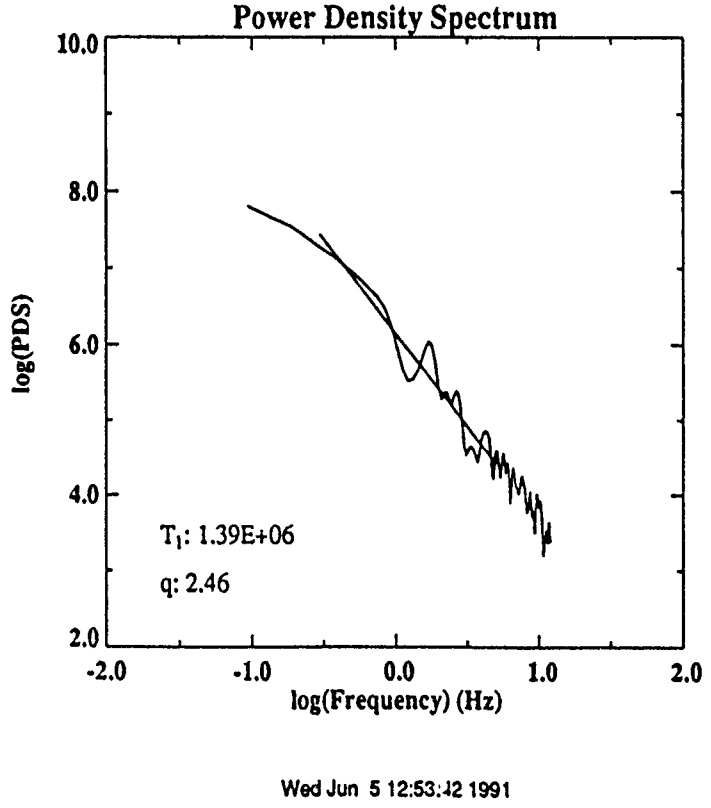

Figure B-3. The same as plot B-1 (SSIES data) for data point no. 2.

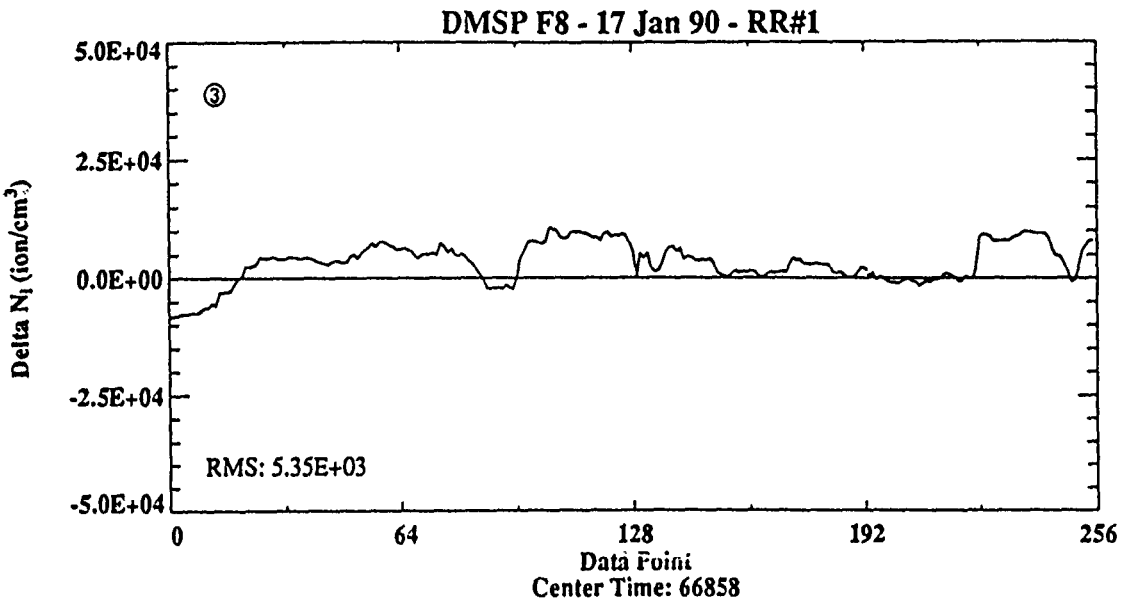

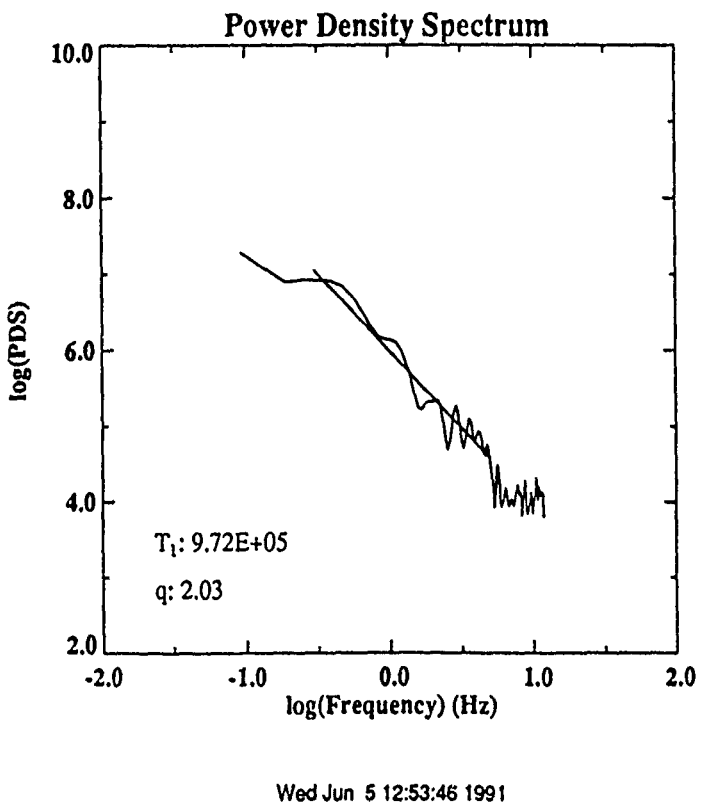

Figure B-5. The same as plot B-1 (SSIES data) for data point no. 3.

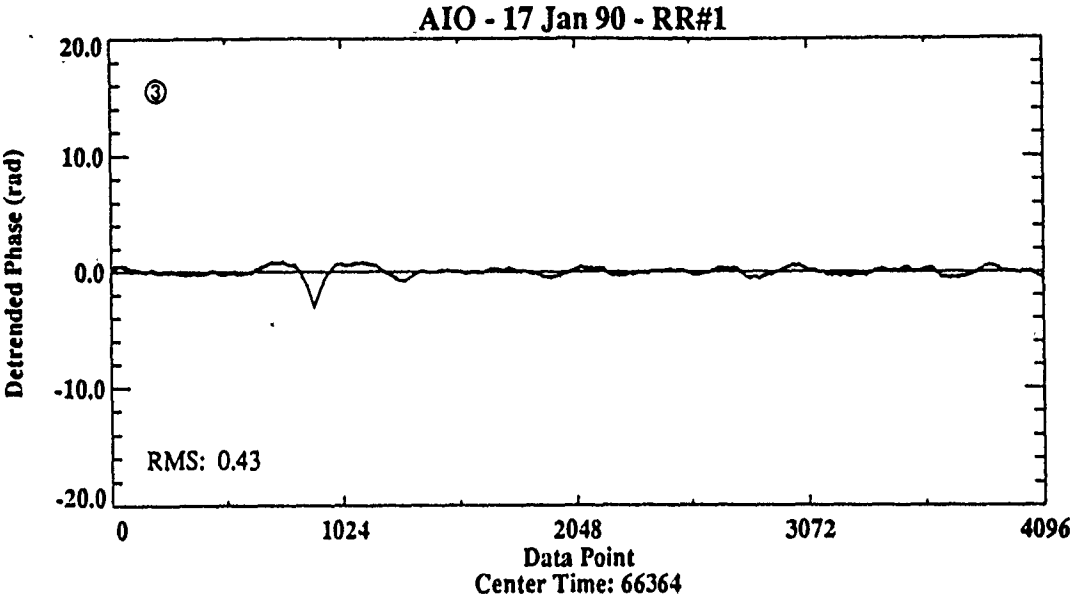

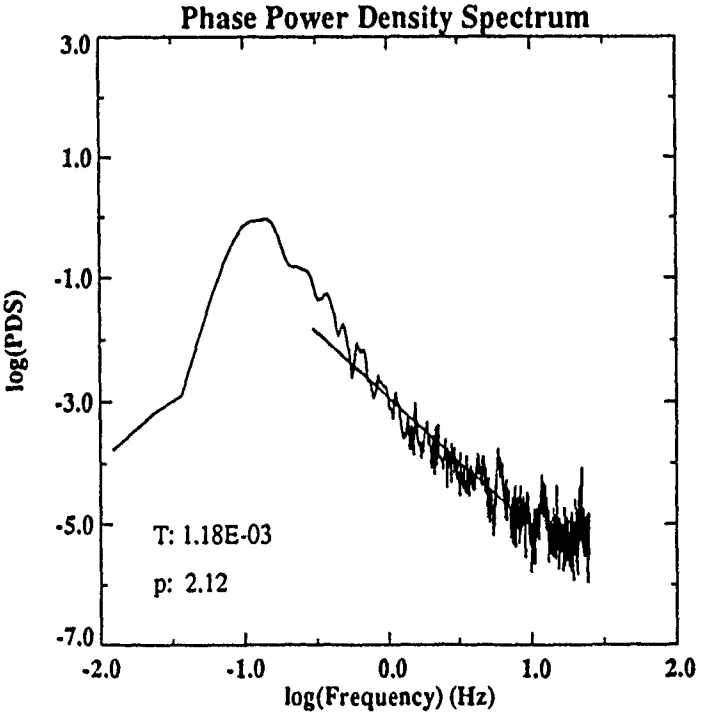

Figure B-6. The same as plot B-2 (AIO-AFSATCOM data) for data point no. 3.

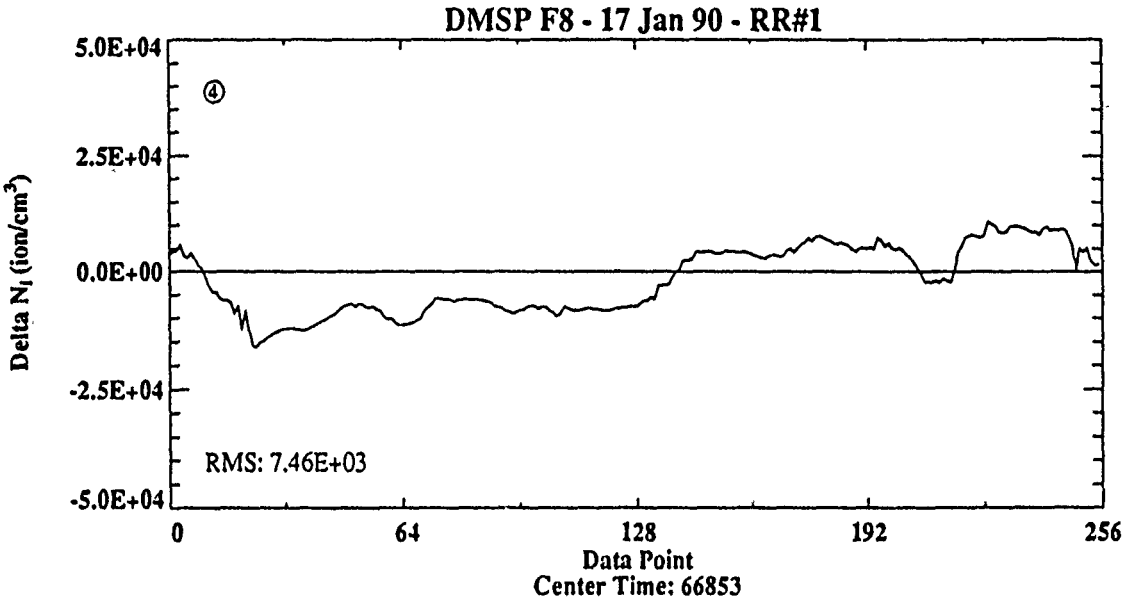

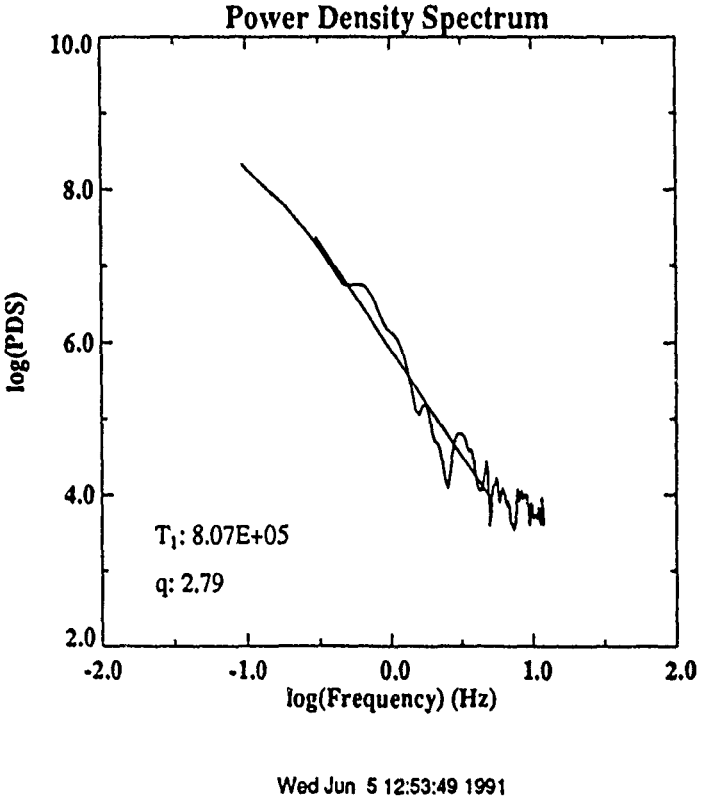

Figure B-7. The same as plot B-1 (SSIES data) for data point no. 4.

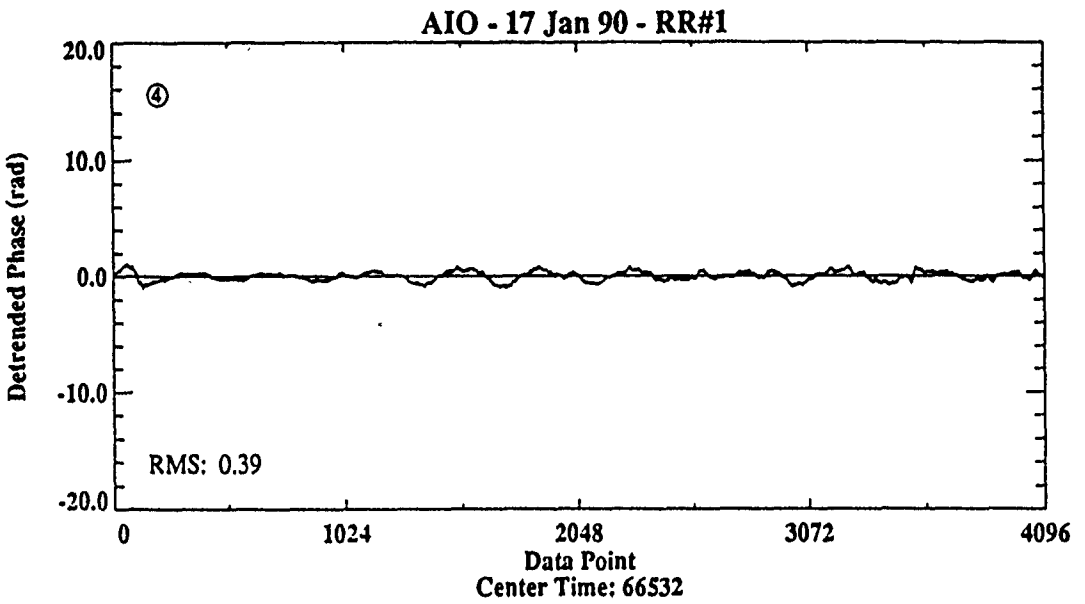

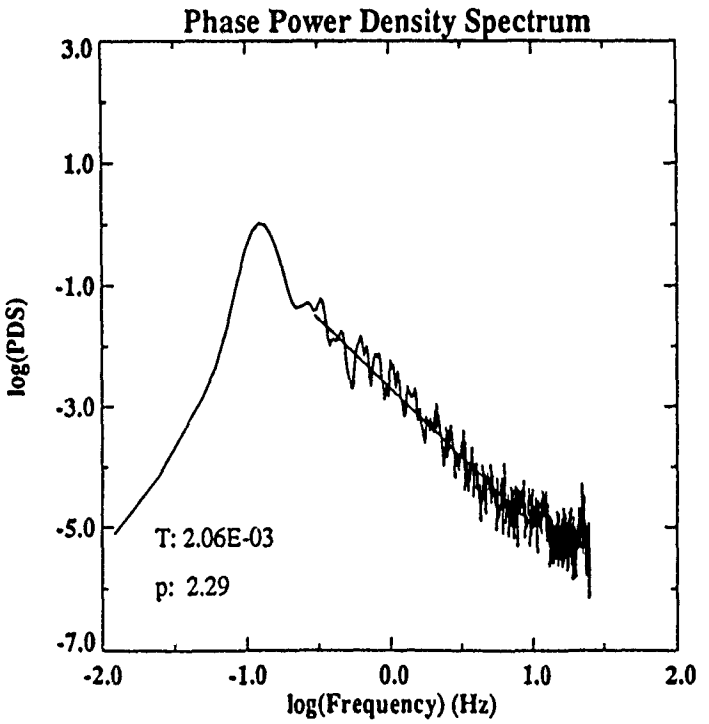

Figure B-8. The same as plot B-2 (AIO-AFSATCOM data) for data point no. 4.

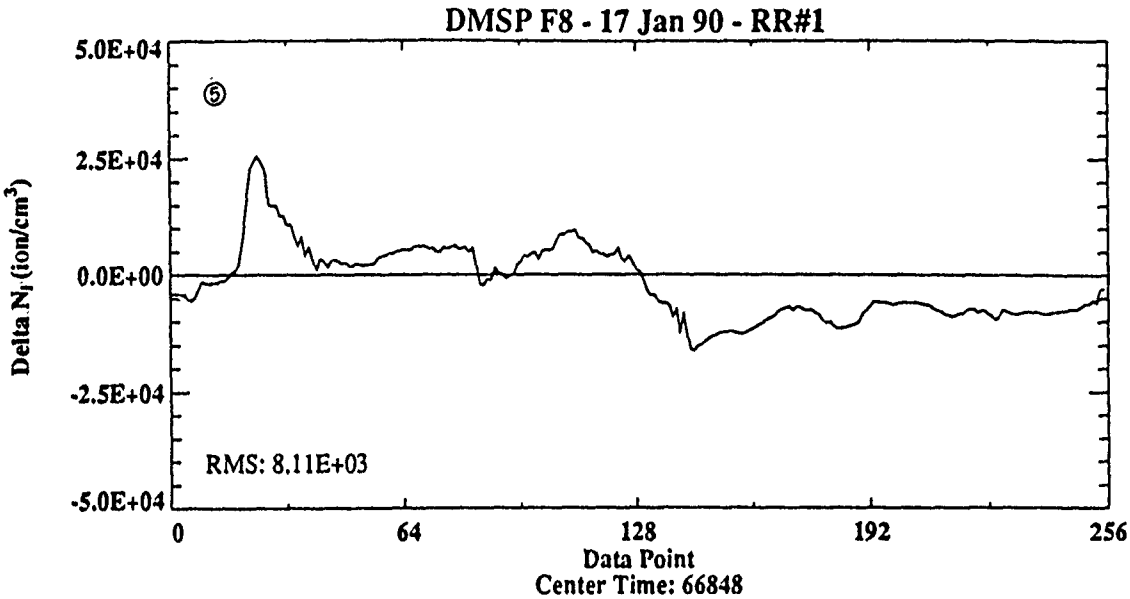

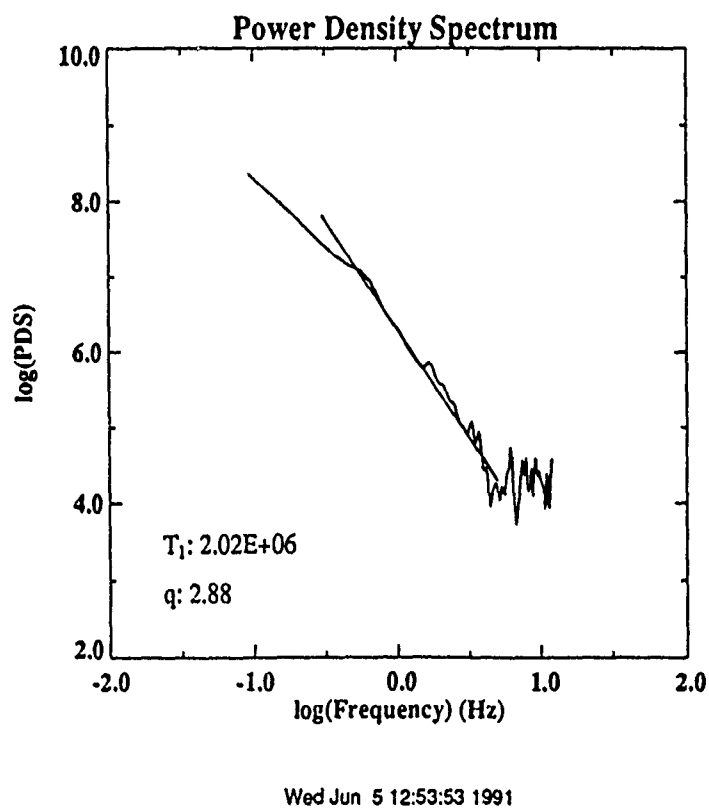

Figure B-9. The same as plot B-1 (SSIES data) for data point no. 5.

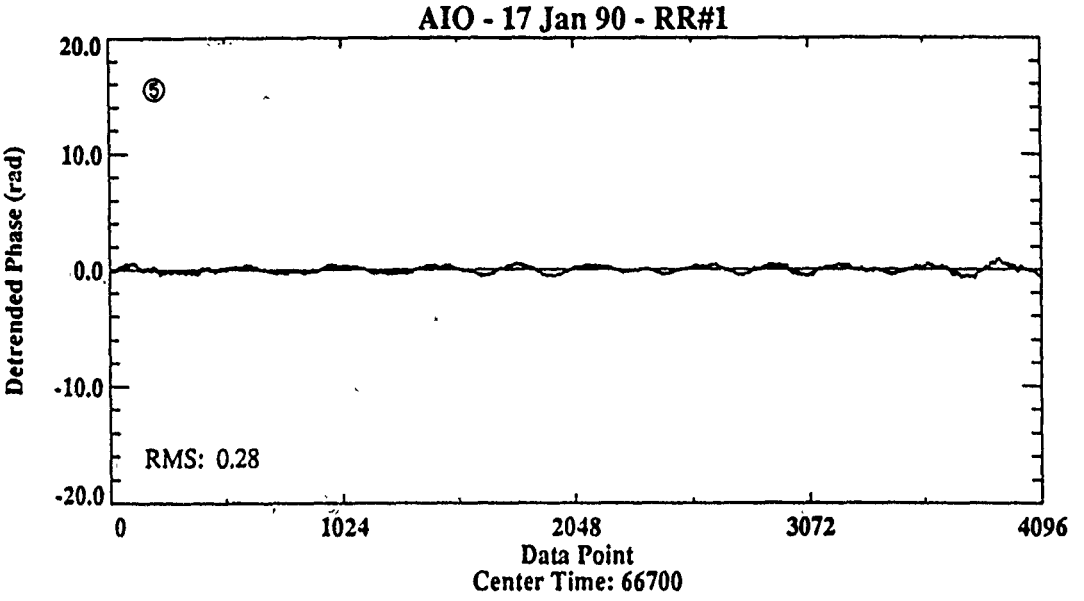

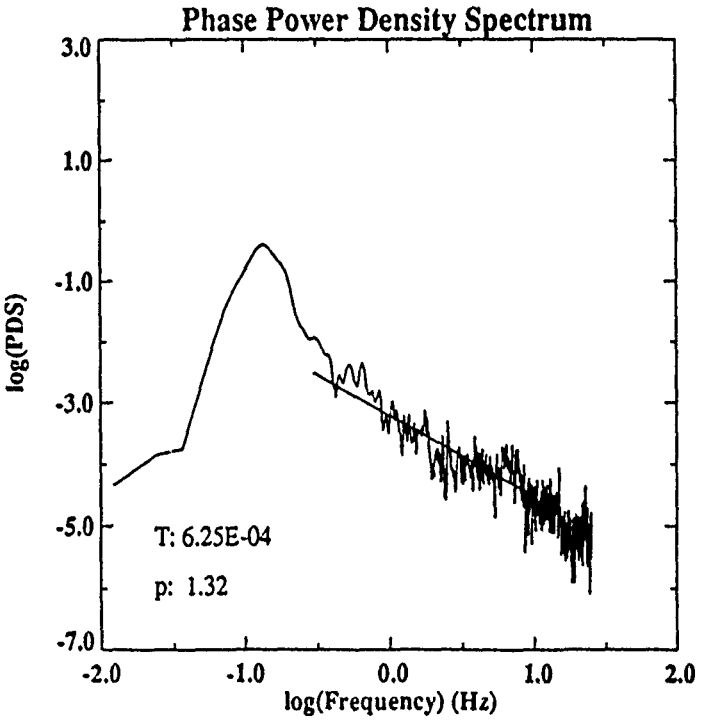

Figure B-10. The same as plot B-2 (AIO-AFSATCOM data) for data point no. 5.

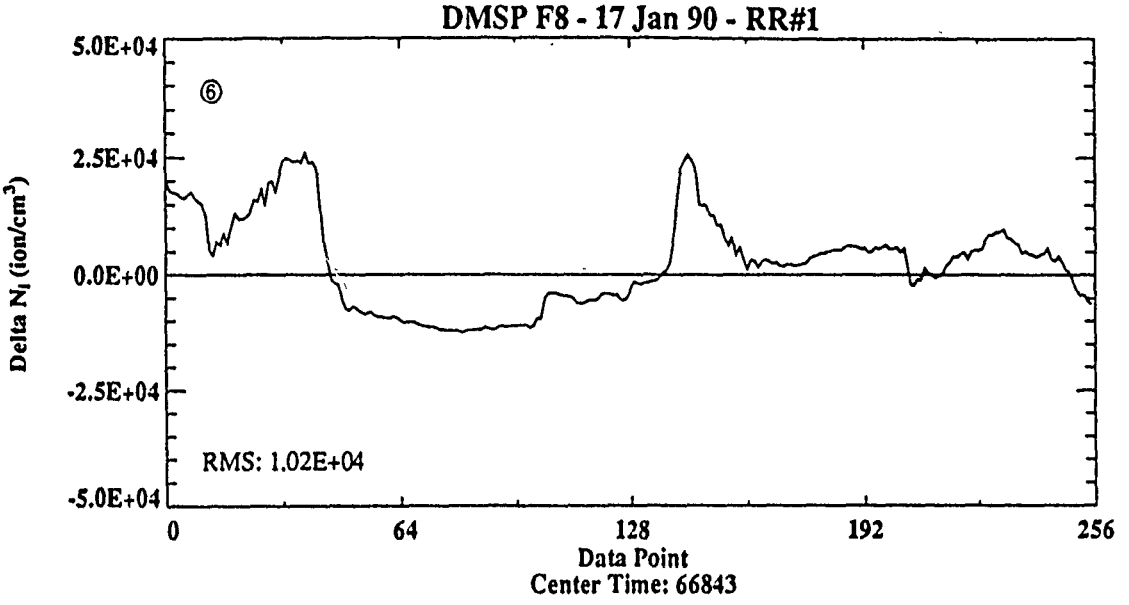

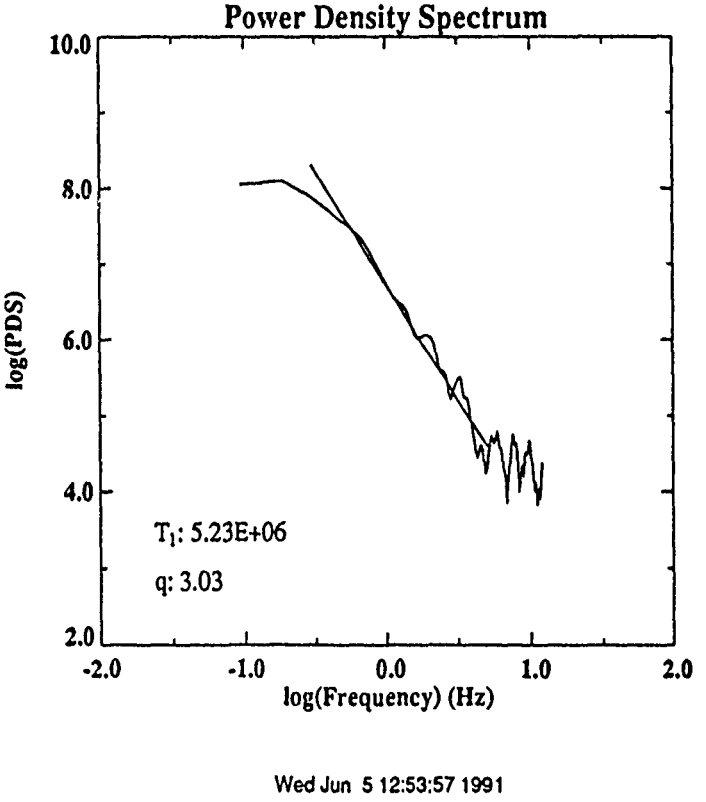

Figure B-11. The same as plot B-1 (SSIES data) for data point no. 6.

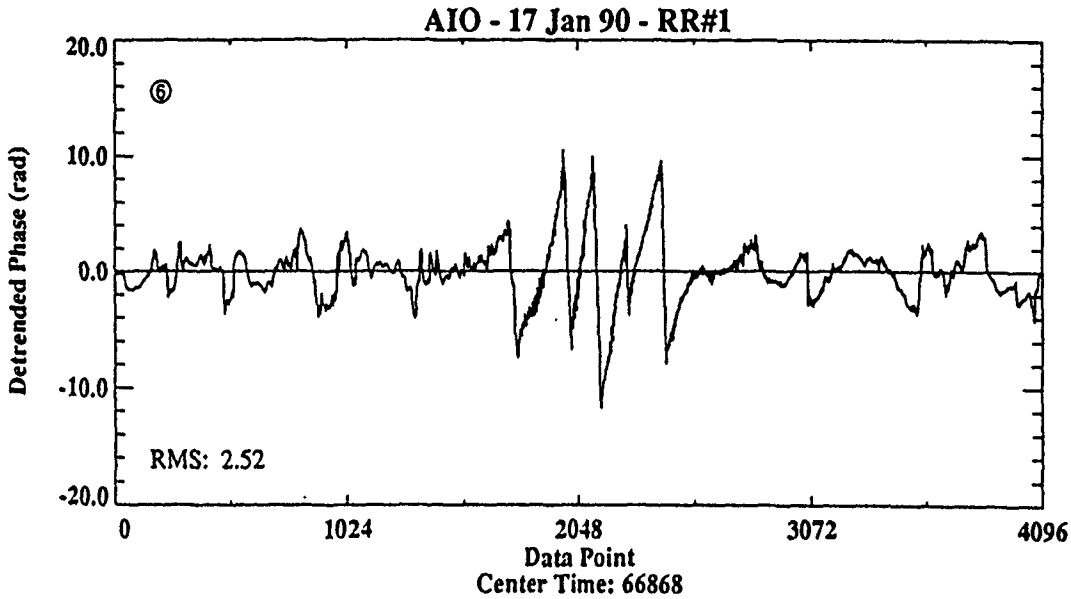

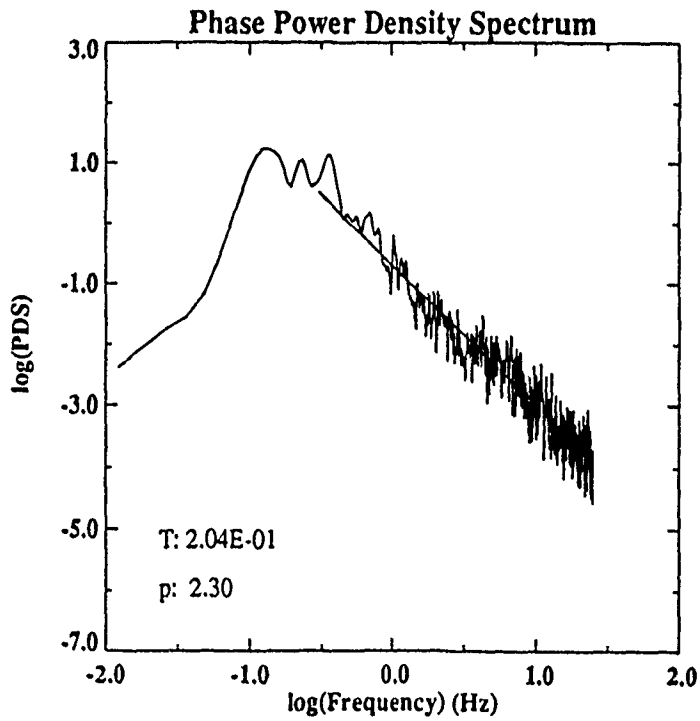

Figure B-12. The same as plot B-2 (AIO-AFSATCOM data) for data point no. 6.

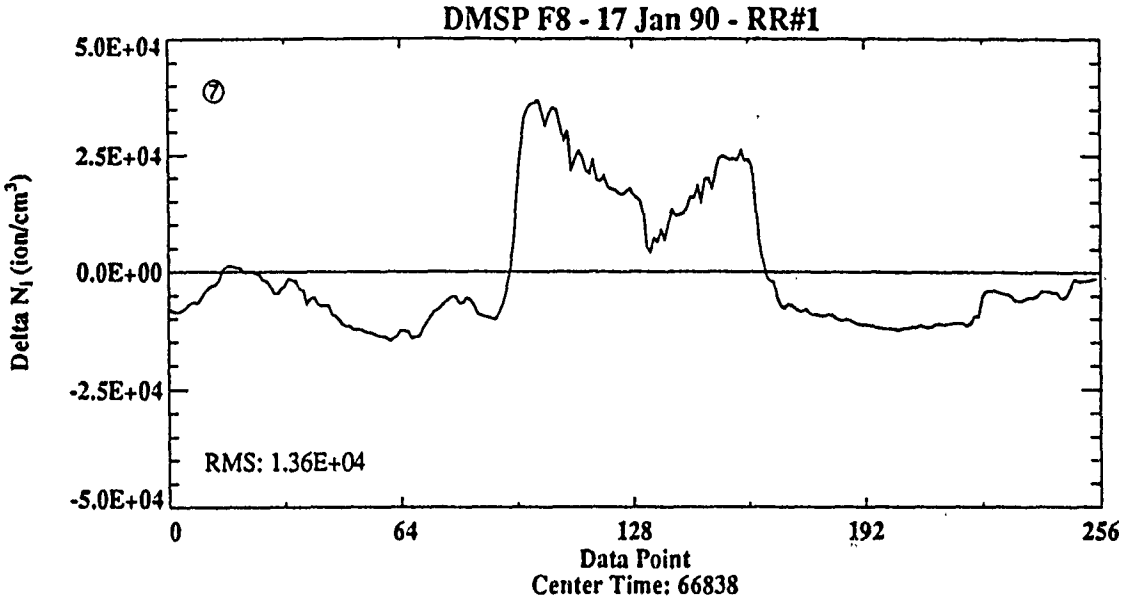

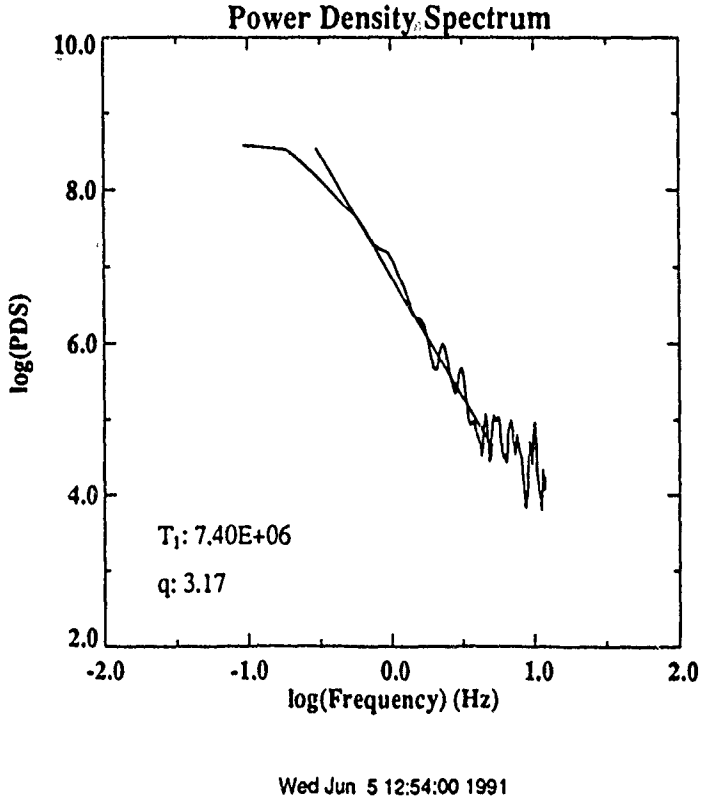

Figure B-13. The same as plot B-1 (SSIES data) for data point no. 7.

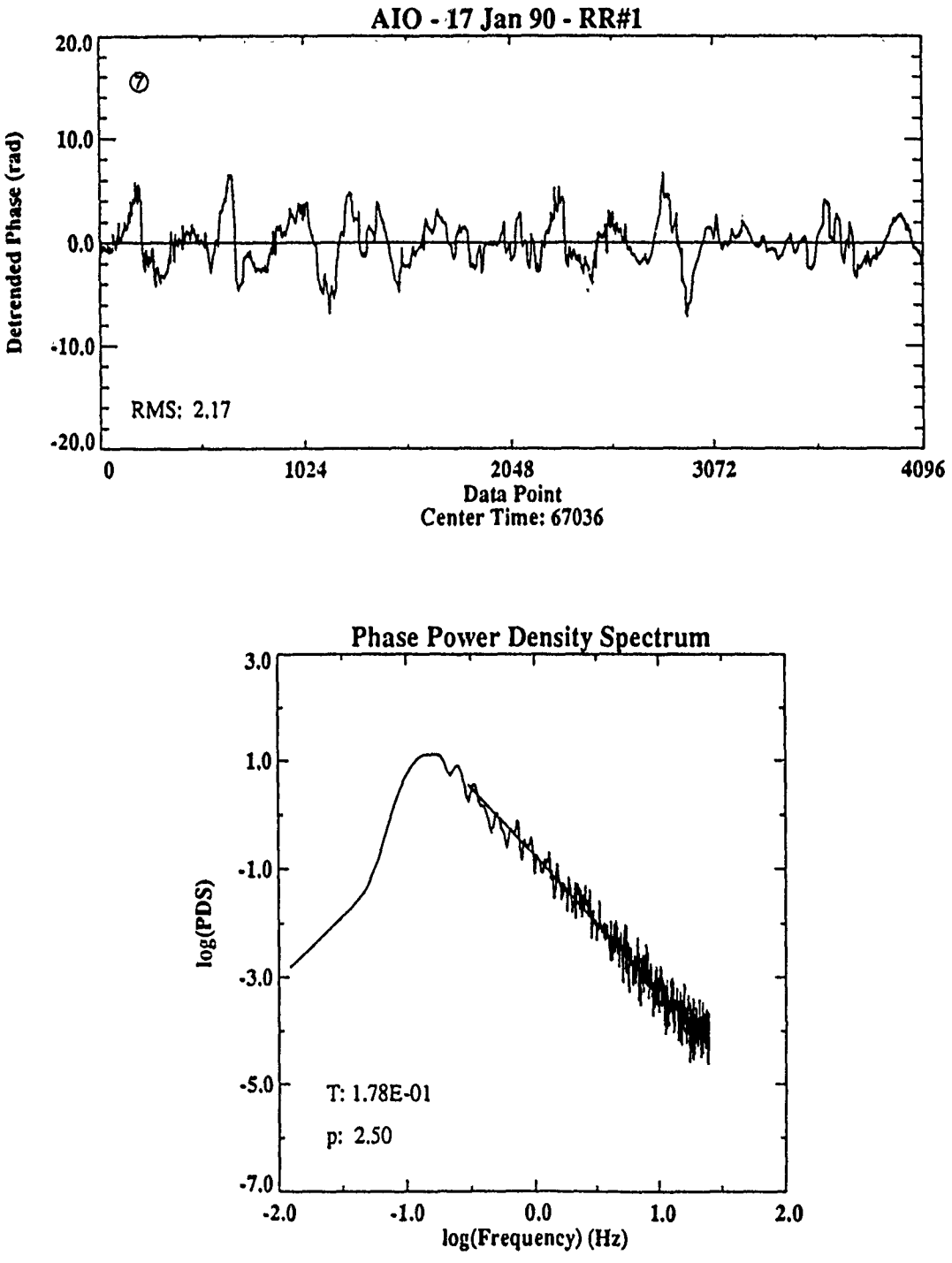

Figure B-14. The same as plot B-2 (AIO-AFSATCOM data) for data point no. 7.

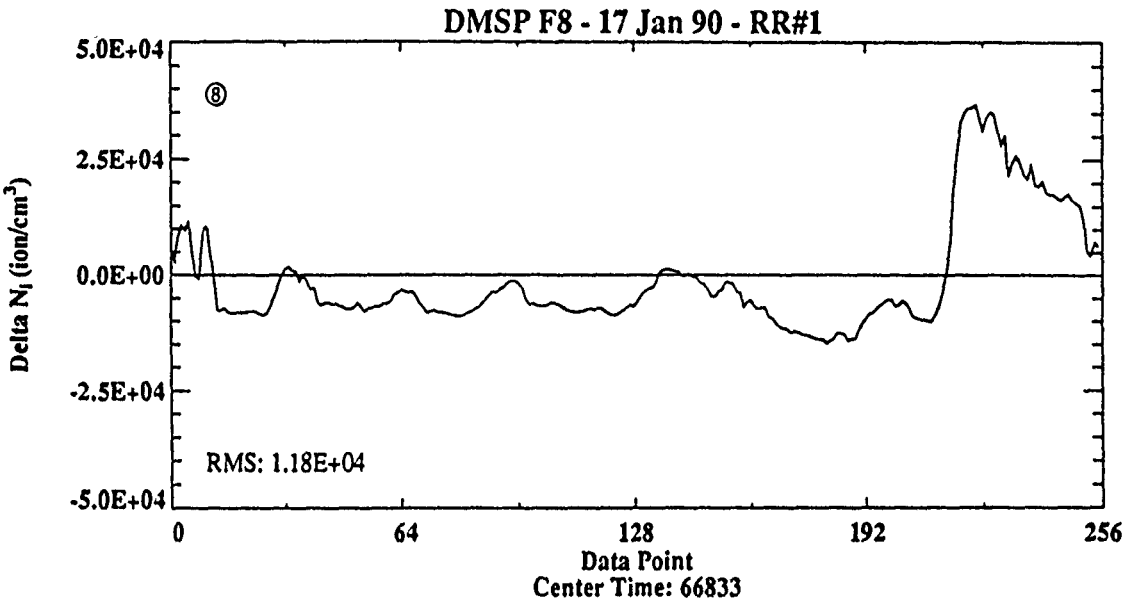

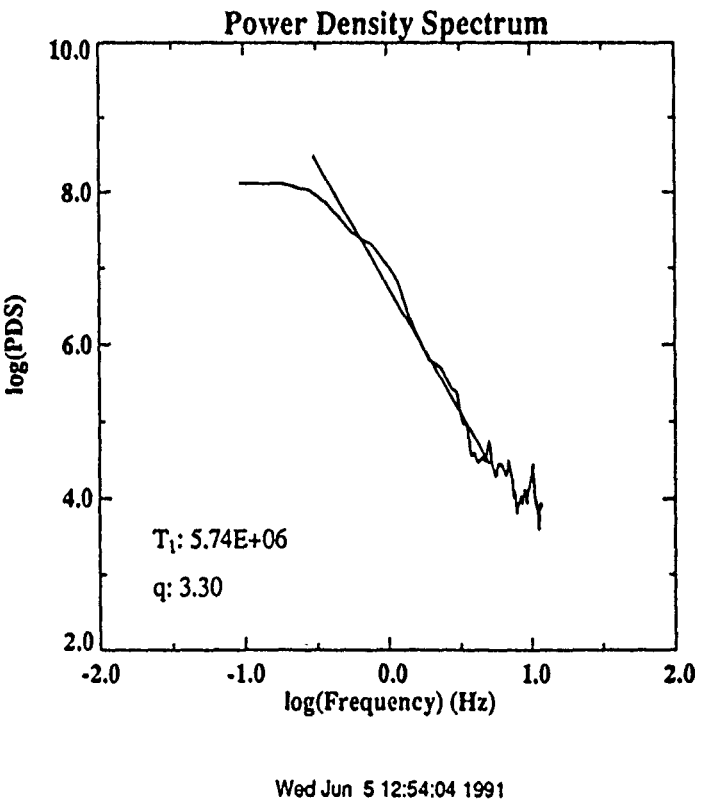

Figure B-15. The same as plot B-1 (SSIES data) for data point no. 8.

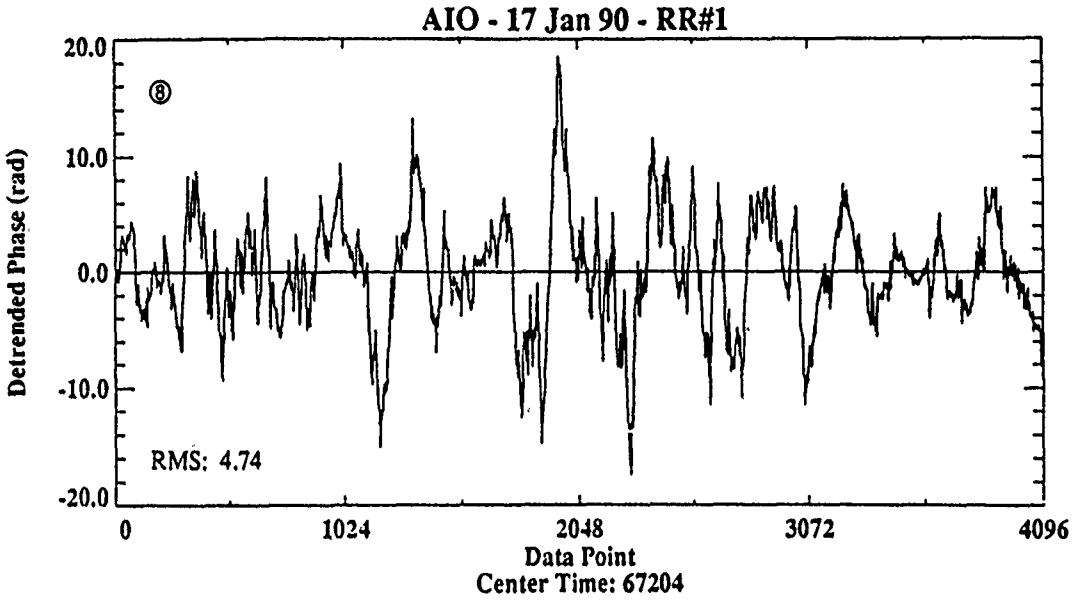

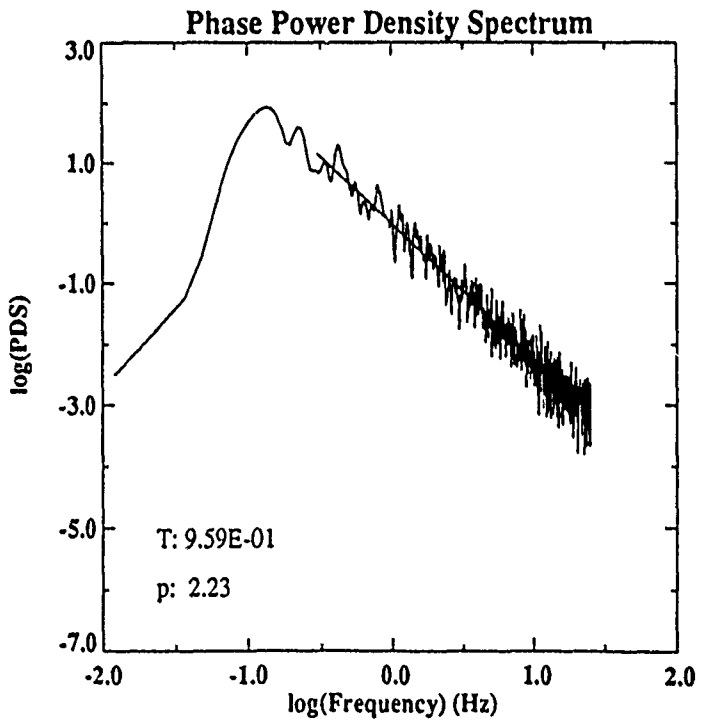

Figure B-16. The same as plot B-2 (AIO-AFSATCOM data) for data point no. 8.

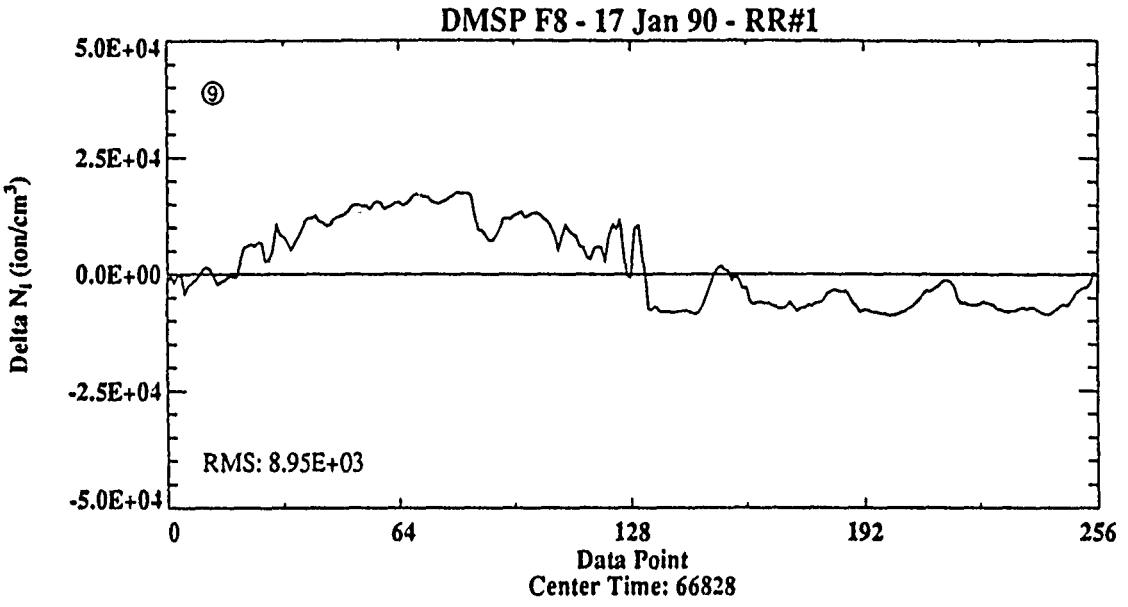

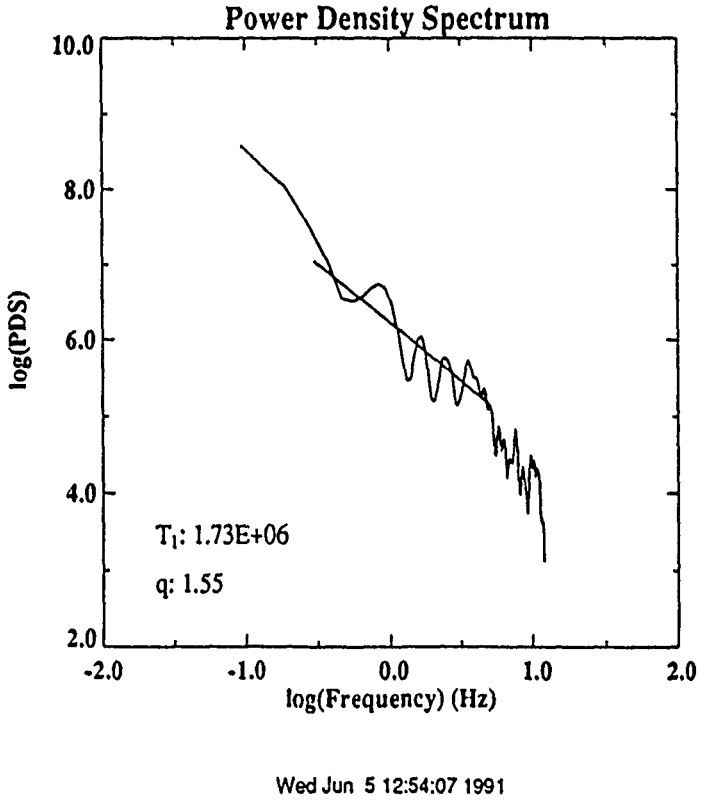

Figure B-17. The same as plot B-1 (SSIES data) for data point no. 9.

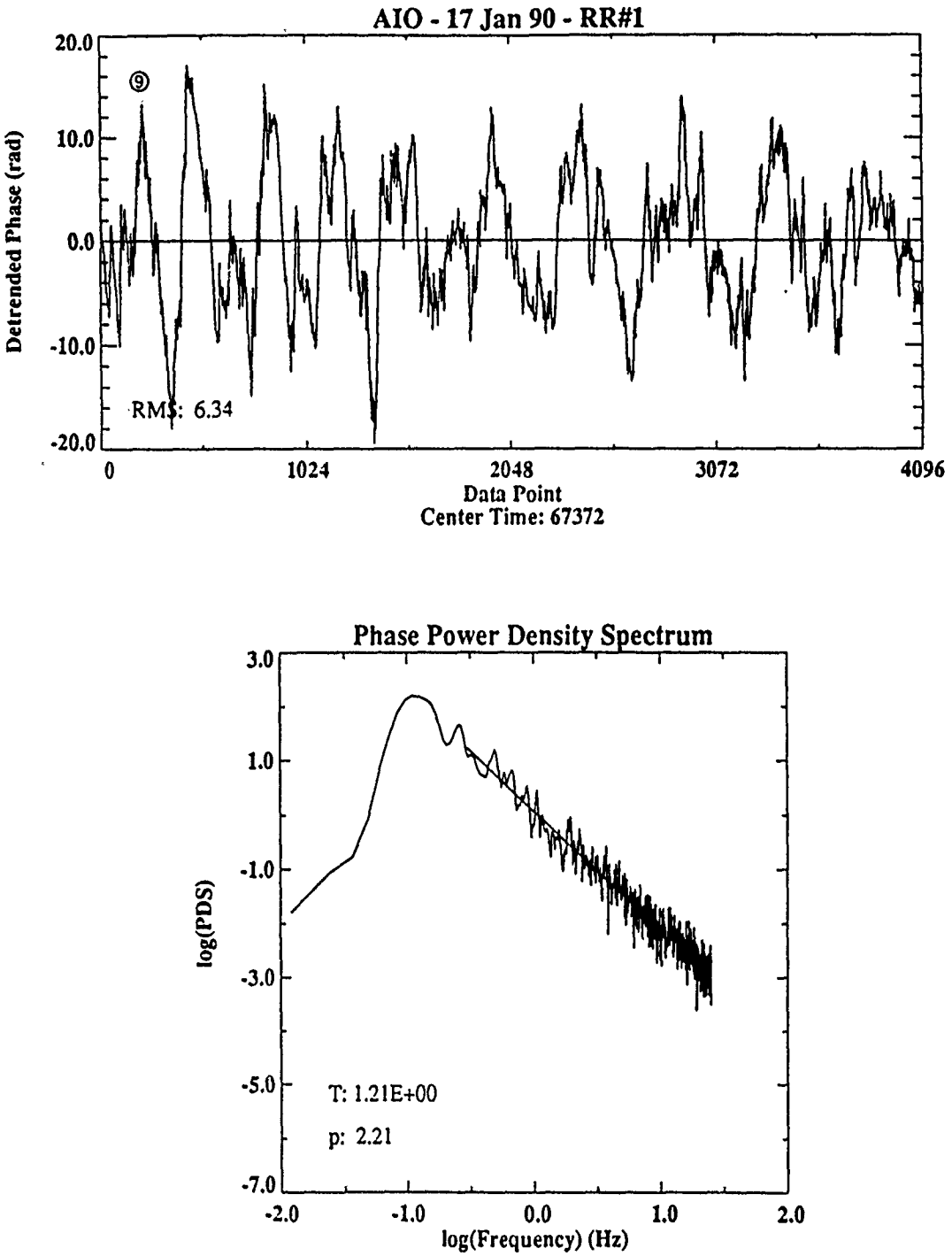

Figure B-18. The same as plot B-2 (AIO-AFSATCOM data) for data point no. 9.